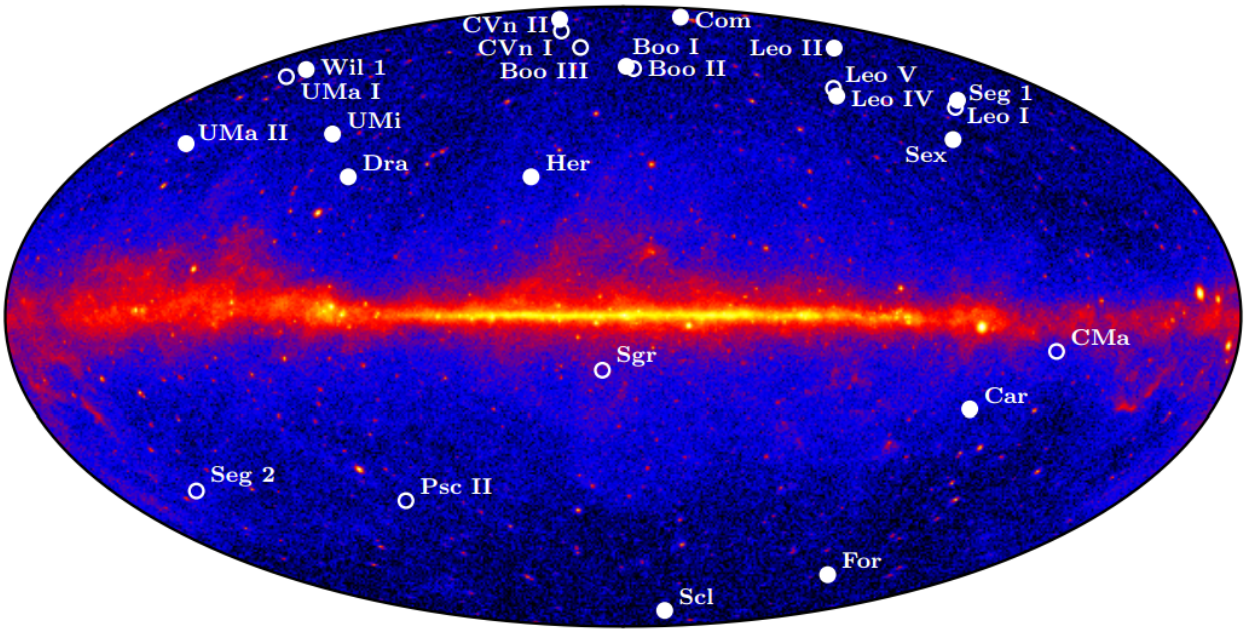

Dwarf Spheroidal J-factors with Self-interacting Dark Matter

A Theoretical and Numerical Analysis of Generalised J-factors for Dark Matter Annihilation in the Satellite Galaxies of the Milky Way

Bachelor's thesis in theoretical subatomic physics

S. Bergström, M. Högberg, E. Olsson, A. Unger

Department of Physics
CHALMERS UNIVERSITY OF TECHNOLOGY
GOTHENBURG UNIVERSITY
Gothenburg, Sweden 2017

Bachelor's thesis 2017:NN

Dwarf Spheroidal J-factors with Self-interacting Dark Matter

A Theoretical and Numerical Analysis of Generalised J-factors for Dark Matter Annihilation in the Satellite Galaxies of the Milky Way

Sebastian Bergström, Michael Högberg,
Emelie Olsson, Andreas Unger

CHALMERS
UNIVERSITY OF TECHNOLOGY

Department of Physics
Division of Subatomic and Plasma Physics
Chalmers University of Technology and Gothenburg University
Gothenburg, Sweden 2017

Dwarf Spheroidal J-factors with Self-interacting Dark Matter
A Theoretical and Numerical Analysis of Generalised J-factors for Dark Matter Annihilation in the Satellite Galaxies of the Milky Way
SEBASTIAN BERGSTRÖM, MICHAEL HÖGBERG, EMELIE OLSSON, ANDREAS UNGER

Supervisor: Riccardo Catena, Department of Physics
Examiner: Jan Swensson, Department of Physics

Bachelor's Thesis 2017:NN
Department of Physics
Division of Subatomic and Plasma Physics
Chalmers University of Technology
Gothenburg University
SE-412 96 Gothenburg
Telephone +46 31 772 1000

Cover: Known dwarf spheroidal satellite galaxies of the Milky Way overlaid on a Hammer-Aitoff projection of a 4-year LAT counts map (E > 1 GeV). Credit goes to Ackermann et al. [1].

Typeset in LaTeX
Printed by [Name of printing company]
Gothenburg, Sweden 2017

Dwarf Spheroidal J-factors with Self-interacting Dark Matter
A Theoretical and Numerical Analysis of Generalised J-factors for
Dark Matter Annihilation in the Satellite Galaxies of the Milky Way
SEBASTIAN BERGSTRÖM, MICHAEL HÖGBERG, EMELIE OLSSON, ANDREAS UNGER
Department of Physics
Chalmers University of Technology
Gothenburg University

Abstract

The next decade of searches in the field of dark matter will focus on the detection of gamma rays from dark matter annihilation in dwarf spheroidal galaxies. This dark matter-induced gamma ray flux crucially depends on a quantity known as the J-factor. In current research, the J-factor calculations does not include self-interaction between the dark matter particles, but there are indications on galactic scales that dark matter is self-interacting. The purpose of this thesis is to introduce a thorough generalisation of the J-factor to include a self-interacting effect and to compute the factor for 20 dwarf spheroidal galaxies orbiting the Milky Way. We thoroughly study the fundamental theory needed to compute the J-factor, based on Newtonian dynamics and non-relativistic quantum mechanics. A maximum likelihood formalism is applied to velocity data from dwarf spheroidal galaxies, assuming a Gaussian distribution for the line of sight velocity data. From this we extract galactic length and density scale parameters. The acquired parameters are then used to compute the J-factor. Using a binning approach, we present an error estimate in J. The used method is compared to previously published results, by neglecting self-interaction. We perform the first fully rigorous calculation for the J-factor, properly taking into account the dark matter velocity distribution. We can deduce that a previously used approximation of the self-interaction overestimates the J-factor by 1.5 orders of magnitude. Furthermore, we confirm that our method produces three to four orders of magnitudes larger values compared to J-factors without self-interaction.

Keywords: dark matter, J-factor, self-interacting, WIMP, annihilation.

Sammanfattning

Det kommande decenniets forskning om mörk materia kommer att fokusera på detektionen av gammastrålning från annihilation av mörk materia i sfäriska dvärggalaxer. Flödet av gammastrålning som uppkommer vid mörk materia-annihilation har ett centralt beroende av en kvantitet som kallas J-faktorn. I nuvarande forskning inkluderas inte självinteraktion mellan mörk materia-partiklarna vid beräkningar av J-faktorn. Det finns dock indikationer på galaktisk skala att mörk materia är självinteragerande. Syftet med den här rapporten är att introducera den första rigorösa generaliseringen av J-faktorn, där effekten av självinteraktion behandlas, och beräkna faktorn för 20 sfäriska dvärggalaxer kring Vintergatan. Vi studerar noggrant den grundläggande teorin som krävs för att beräkna J-faktorer, baserat på Newtonsk dynamik och icke-relativistisk kvantmekanik. En maximum likelihood-skattning används på data från dvärggalaxer, under antagandet att hastigheten för stjärnorna följer en Gaussisk distribution. Från detta extraheras parametrar för längd- och densitetsskalan hos galaxen. De erhållna parametrarna används sedan för att beräkna J-faktorn. Genom att använda en sållningsmetod beräknas en feluppskattning i J. Maximum likelihood-metoden tillämpas på fallet utan självinteraktion för att jämföra med tidigare studier. Vi utför en utförlig beräkning av J-faktorn där hänsyn tas till den mörka materians hastighetsdistribution. Slutsatsen dras att en tidigare använd uppskattning överskattar J-faktorn med 1.5 storleksordningar. Dessutom kan vi bekräfta att vår metod ger tre till fyra storleksordningar större värde för J-faktorn jämfört med utan självinteraktion.

Nyckelord: mörk materia, J-faktor, självinteraktion, WIMP, annihilation.

Acknowledgements

We are very thankful to our supervisor Riccardo Catena, without whom this bachelor project had not been possible. He has been a mediator of several fundamental non-SM forces; providing us with the theoretical material, the velocity data and the overall knowledge to solve this task, not to mention his professional expertise in scientific writing. A special thanks to the other group working on the same project, Magdalena Eriksson, Björn Eurenius, Susanna Larsson and Rikard Wadman. They have been a great support throughout the process with discussions on widely different physics concepts as well as fika buddies. It has been absolutely invaluable to be able to compare data with them when conducting new calculations.
We also want to thank Andrea Chiappo for sending the data of the 20 dwarf spheroidal galaxies.

S. Bergström, M. Högberg, E. Olsson, A. Unger

Gothenburg, May 2017

Contents

List of Figures

List of Tables

1

Introduction

For a long time dark matter has been an elusive concept. The idea of some unperceivable cosmic object has fascinated humans ever since the time of the ancient Greeks. Up until the end of the twentieth century it was believed we could not observe the dark matter, thought to be made of faint stars, because of our lack of technology. Today, we know that dark matter does not emit radiation at all [2].

Dark matter is extensively studied since it explains a wide variety of astronomical phenomena from galactic to cosmological scales [2]. One example is the discrepancies in galactic rotation curves of disc galaxies. Assuming a dark matter halo explains this discrepancy [3]. It should be noted that this problem also can be solved with an adjustment of the theory of gravity, known as Modified Newtonian Dynamics [4]. However, for many other phenomena, dark matter is the only plausible explanation. Examples of such are the collision of galaxies in the Bullet cluster and the large-scale structure of the universe [5, 6].

Dark matter is assumed to consist of a new hypothetical particle outside the standard model. Apart from its' gravitational interaction, this particle interacts at most weakly with ordinary matter. One of the most promising candidates for dark matter today is the Weakly Interacting Massive Particle (WIMP) (see [7] or [8]). Furthermore, non-relativistic WIMPs have the strongest scientific support [2].

The annihilation, or decay, of WIMPs is assumed to generate gamma ray photons, among other standard model particles. This is the principle for indirect detection of dark matter. The photon flux from WIMP annihilation in dwarf spheroidal galaxies (dSph) and the galactic centre can be measured, and a key part of this flux is called the J-factor. This J-factor has been computed for the Milky ways' dwarf satellite galaxies in previous research [9].

Even though cold WIMPs are the most promising candidate for dark matter, it can not explain all phenomena. One of the most significant is the "Cuspy problem" [10]. This can be solved by introducing the property of self-interaction for WIMPs. Such an interaction alters the annihilation rate of WIMPs and in turn the J-factor.

The aim of this thesis is to generalise the J-factor to include self-interacting WIMPs. The self-interaction will be introduced as a Yukawa potential [11]. The theoretical formalism will be based on Newtonian dynamics and non-relativistic quantum mechanics. A likelihood estimation of the generalised J-factor will be done for 20 dSphs of the Milky Way. An error estimate to the J-factor will also be included.

2

Background

In this chapter we present the theoretical background for both dark matter and the presumed dark matter particles. Also, this chapter includes a brief review of the current research on dark matter, especially J-factors. The last section is an introduction to some astrophysical concepts needed for the derivations in chapter 3.

2.1 Evidence for dark matter

Today, it is believed that 26% of the universe consist of dark matter, compared to 5% ordinary matter [6]. It should also be mentioned that the rest is another concept called dark energy, which has been introduced to explain the accelerating expansion of the universe. Dark energy does not have matter properties and should not be confused with dark matter, even though they share a similar name.

The evidence for dark matter is today compelling. To begin with, the dynamics of galaxy clusters would simply fall apart without the additional gravity from dark matter. It is also needed to explain the velocity dispersion in galaxy clusters. In the first half of the twentieth century the astronomer Fritz Zwicky, one of the great pioneers in the field of dark matter, calculated that the velocity dispersion of the galaxies in the Coma Cluster without some form of invisible matter would be 10 times smaller than the observed dispersion [2]. Another piece of evidence for dark matter is the shape of the galactic rotation curves, where the velocities for the stars remain constant as distance from the galaxy's centre increases. In theories without dark matter, the velocities should behave precisely as in our own solar neighbourhood where the orbital velocity of the planets decrease with distance from the sun [3]. This indicates a smoother mass distribution than the one for the visible mass which is clearly larger at the galactic centre. A halo of dark matter would explain the constant velocities.

An additional example is the collision between two galaxies in the Bullet Cluster [5]. Astronomers who worked on the Hubble Space Telescope observed the collision where the galaxies' centres merged. When comparing data based on optical observations with data based on gravitational lensing they found an inconsistency. Dark matter could explain this inconsistency, since it only influences ordinary matter gravitationally but very rarely collides with it. The ordinary matter will bounce

in the collision, whereas the dark matter slips through smoothly. Also, dark matter explains the extent of gravitational lensing observed.

Dark matter is also needed to explain the formation of the universe. The Cosmic Microwave Background (CMB) is electromagnetic radiation remaining from the recombination, when the first atoms formed and light could propagate through the universe. This radiation is almost isotropic, but shows faint patterns, which were established when gravity pulling in and photon pressure pushing out caused oscillations. Dark matter changes this pattern dramatically, since it is only affected gravitationally and not by the photon pressure [6]. Without dark matter these oscillations would prevent the formation of any lumps, and the large structure formation we observe today in the universe would not have been possible. Instead, the dark matter gets a head start when it comes to forming dense regions, and such simulations matches the distribution of galaxies and clusters we observe today.

Even though the evidence for dark matter is well established, there are a number of theories about what dark matter actually is. One of the best candidates as of today is the weakly interacting massive particle (WIMP), although many other candidates exists. This particle might also fit the hypothesis of self-interaction very well, and is the main focus of this study.

2.2 Why self-interacting WIMPs?

There are several reasons for considering the WIMP as a dark matter candidate. First of all, if dark matter has a *particle* nature it could explain the observed gravitational effects. Also, the observed flux of photons from many galaxies is today higher than the expected flux from the luminous matter. Annihilating dark matter particles would explain this.

The reason for considering *massive* dark matter particles is because their mass has to match the desired gravitational potential, without being numerous enough to annihilate into other kinds of particles or energy. The particles need to be *weakly interacting* with normal matter because the effects of dark matter has yet only been seen in terms of gravitational effects and not by any other kind of interaction. If dark matter particles interacts through any other SM force with ordinary matter, this interaction must be by the weak force.

Furthermore, it has been found that dark matter consisting of WIMPs moving with non-relativistic velocities, often denoted as cold particles, most accurately agree with simulations of the formation of the early universe [2]. In the early universe the temperature was a lot higher, and consequently the energy sufficient for the WIMPs to both annihilate into and form from lighter particles. When the universe cooled, the thermal energy of the lighter particles were no longer high enough to form WIMPs through annihilation. The amount of WIMPs decreased exponentially, since they could still annihilate into lighter particles, until the number density were low enough for the annihilation to cease at large. The number of WIMPs today is therefore approximately constant [7]. The low velocities will make the WIMPs

clump together in clouds, since they can not overcome their mutual gravitational force.

A particle with larger cross section (i.e. the probability for the annihilation to occur) will in this model end up with a smaller number density, because it will annihilate for a longer time. For dark matter, a cross section about the size of the weak nuclear force would match the amount of WIMPs left in the Universe. A weakly interacting particle with that annihilation cross section and a mass around 100 GeV is suggested by the supersymmetric extension of the standard model. This coincidence is often referred to as the "WIMP miracle"

The WIMP is assumed to be its own antiparticle and one WIMP can therefore annihilate with any other WIMP. The high-energy photons (and other SM particles) produced in such an annihilation can be detected on Earth. However, even if annihilating WIMPs and luminous matter is considered, the observed flux of photons from galaxies will be higher than the calculated amount [12]. Introducing self-interacting WIMPs might equalise this relation, since it would increase the annihilation rate and in turn the flux of photons from the galaxies.

There is a variety of different models deciding both the WIMPs mass and the mass of the mediator particle for the self-interaction. The strength of the interaction depends on the mass of the mediator particle. The current limit of the self-interaction cross section is $\sigma/m < 2.23 \cdot 10^{-24}$ cm^2/GeV [13]. The dark matter mass is in the range 1 GeV - 100 TeV. In this thesis we use a model which assumes that dark matter annihilations is the origin of the whole discrepancy between observed and theoretically calculated flux of particles, which actually can originate from other sources. The WIMP is thought to have a mass around 500-800 GeV and the mediator particle of the self-interaction a mass of 1 GeV [8]. The WIMP is then heavier than the SM particles, and therefore one can get a various number of different particles from the annihilation.

Introducing self-interaction might also solve other cosmological problems. One of the most impactful unsolved problems is known as the "Cuspy problem". This problem addresses a discrepancy between observed dark matter densities and simulations. Simulations proposes cusped density profiles that diverges for small radii, in contrast to the observed ones that flatten out; so called cored profiles [14, 15]. When simulations of the mass of the dSphs are compared to observations, it is found that the dSphs around the Milky Way should be more massive than observed. This is known as the "Too big to fail problem" and is also solver with self-interacting WIMPs.

Another problem is that the number of satellite galaxies is a lot lower than the expected amount given from simulations, which is called the "Satellite problem". All these problems can be solved by introducing self-interacting dark matter [10]. With a self-interaction the WIMPs will not be able to clump together as much, since then they would annihilate more efficiently. This will change the halo density and make it smoother. As an effect, the mass for the simulated dSphs will decrease and also the number of substructures.

Hence, there is a clear support of dark matter consisting of self-interacting WIMPs. The reasons mentioned in this section are also the reasons for this study to perform calculations based on self-interacting dark matter.

2.3 Current research and J-factors

Current research in astroparticle physics primarily focuses on detecting dark matter particles from the cosmos and understanding their nature. Experiments search for photons, charged antimatter or neutrinos produced in dark matter annihilation or decay. The search is performed in dark matter dominated astrophysical objects, such as dSphs or the galactic centre. Detection strategies can be divides into two complementary approaches, known as direct and indirect detection. Direct detection experiments search for nuclear recoil events induced by the scattering of Milky Way dark matter particles in low-temperature detectors.

Indirect detection is based on the annihilation between dark matter particles. As mentioned before, such annihilation produces standard model particles which can be observed, particularly photons. To draw conclusions of the particle nature of dark matter, one can compare the measured production of gamma rays in some region in space with the theoretical value based on the number of stars emitting light in that region. This thesis will contribute to the calculations of the flux of photons originated from this dark matter particle annihilation.

The indirect dark matter searches are mostly based on observations of dSphs orbiting the Milky way. The reason for this is the high proportion of dark matter relative to ordinary matter in these galaxies and their symmetric near spherical shape. It is for these reasons that star velocity data from a number of dSphs is the basis for our calculations.

In order to perform indirect searches, one must know the flux of particles originating from dark matter particle annihilation. The flux, Γ, of a certain particle is proportional to the annihilation rate of dark matter. Γ is often expressed as a differential rate over energies:

$$\frac{\mathrm{d}\Gamma}{\mathrm{d}E} \propto \int_{\Delta\Omega} \int_{\mathrm{l.o.s.}} \langle \sigma v \rangle \rho_{\mathrm{DM}}^2 \, \mathrm{d}s \, \mathrm{d}\Omega, \tag{2.1}$$

where $\langle \sigma v \rangle$ is the mean velocity cross section, ρ_{DM} is the dark matter density and $\Delta\Omega$ is the solid angle subtended by the stellar region, in our case a small galaxy orbiting the Milky Way (a dSph), as seen from the Earth. For a full description of the flux, the branching ratio (a particle physics factor) should be included in equation (2.1), but a proper description of that is outside the scope of this thesis (consider instead Ferrer et al. [16]).

If the velocity averaged cross section, $\langle \sigma v \rangle$, is constant throughout the galaxy, it can be taken out of the integral. This is the case when the product σv is velocity independent, which it is for the s-wave annihilation of self-interacting dark matter

particles [17]. We denote the constant velocity averaged cross section by $\langle \sigma_0 v \rangle$. Then one retrieves the so called J-factor for the galaxy, defined as

$$J = \int_{\Delta\Omega} \int_{\text{l.o.s.}} \rho_{\text{DM}}^2 \, \mathrm{d}s \, \mathrm{d}\Omega. \tag{2.2}$$

By introducing a J-factor, the annihilation rate in eq. (2.1) can be fully separated in an astrophysics and a particle physics part, corresponding to the J-factor and $\langle \sigma_0 v \rangle$ respectively. Thus, calculating the J-factor for different dSphs is relatively straightforward. It can be done using a maximum likelihood estimation as proposed by Chiappo et al. 2016 [9], which also will outline the approach in this thesis with some minor modifications.

Self-interaction between particles is introduced by adding a potential to the Schrödinger equation describing the particle annihilation. Most commonly, this is done with a Yukawa potential, which will be discussed later. This will introduce a velocity dependence in the product σv and as a result $\langle \sigma v \rangle$ becomes non-constant throughout the galaxy. The simplification leading up to equation (2.2) is then no longer possible. However, this velocity dependence can be encapsulated in what is called a Sommerfeld enhancement factor, $S(v)$, where $\langle \sigma v \rangle = \langle S(v) \sigma_0 v \rangle$. This will be described in more detail in section 3.5. The factor $\sigma_0 v$ is now actually independent of velocity, and thus also of position in the galaxy and can be factored out of both the average and the integral in the same fashion as the simplification leading to (2.2). The new J-factor accounting for self-interaction will now include both astrophysics and particle physics. In this thesis we define this as:

$$J_\ell = \int_{\Delta\Omega} \int_{\text{l.o.s.}} \rho_{\text{DM}}^2 \, \langle S(v) \rangle \, \mathrm{d}s \, \mathrm{d}\Omega. \tag{2.3}$$

Note that for non self-interacting dark matter the Sommerfeld factor is unity, so the expression in (2.3) can be taken as a general expression valid in either case. We denote this new factor J_ℓ, where $\ell = s, p, d, ...$ is the spectroscopic notation for the value of the orbital angular momentum quantum number ℓ used when solving the Schrödinger equation describing the annihilation.

2.4 Astrophysics

In order to present the necessary theoretical framework for this report, a review of some basic astrophysics must be done. In this section we present important definitions and concepts and discuss some of the approximations that are made.

We define a *galaxy* to be an isolated stellar system. That is, the galaxy is bound by its own gravitational force, the stars in the galaxy experience no notable gravitational pull from other galaxies and collisions between galaxies are extremely rare.

The dynamics inside galaxies, as large systems consisting of many individual particles (stars), can generally be described using statistical mechanics even though the

galaxy is far from a gas. This approach is very useful, and often necessary, as it would be impossible to fully describe systems of millions of stars using only Newton's equations. However, this must not be interpreted as stars generally behaving in the same way as, for example, gas molecules. In a gas, the particles do not over long range at all, but instead interact strongly as they come close to each other. This is known as collisions and causes rapid acceleration of particles. In contrast, consider a star in a galaxy. The gravitational force from surrounding stars indeed decreases with the distance as r^{-2} as per Newton's law of gravitation. But, the amount of stars extorting gravitational pull on the very same star increases with distance as r^2, cancelling the decrease in gravitational strength. This is illustrated in figure 2.1. As such, in galaxies the long range interaction are also of importance. This implies that the motion of stars are dictated by the structure of the galaxy as a whole, rather than locally. One say that the dynamics in a galaxy is determined by the *large-scale gradient* in the star density.

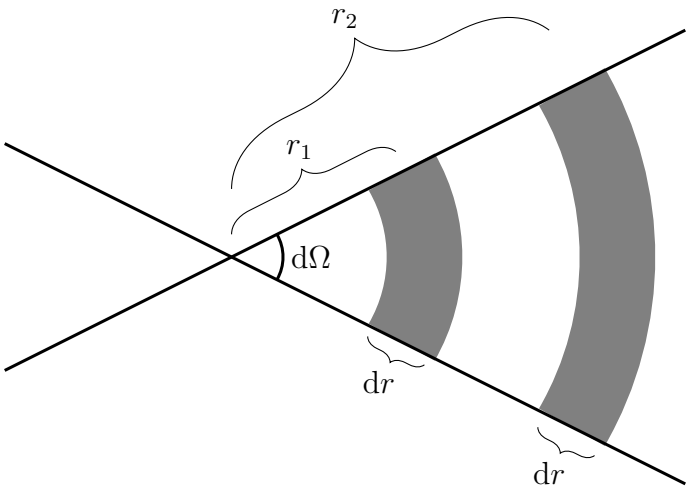

Figure 2.1: The stars in each of the grey segments, at radius r_1 and r_2, acts with the same net force on a star located where the lines intersect if the density of stars is uniform. This can be understood by comparing the gravitational force which decreases as r^{-2} with the amount of stars in the segments which in three dimensions is proportional to r^2. These two contributions cancel out which results in the same net force.

However, it is not always enough to consider the large-scale gradient in the star density. Consider a star travelling through a galaxy. If the star encounters another star very close on, its course will be somewhat perturbed from the description given by the large-scale gradient in the star density. That is because the motion resulting from the encounter is highly dependent on the exact positions of the two stars. If the perturbation is small compared to the unperturbed velocity, one can define the *relaxation time*, τ_{relax}, as the time it takes for the total perturbation in the star's velocity from multiple encounters to be of the same order as the velocity would have been without the perturbation [18]. This perturbation of a star's velocity during one crossing of the galaxy depends on how many stars it encounters.

For a galaxy younger than the time it takes for a star to cross the galaxy, or a larger galaxy with less stars, the stars has not been significantly perturbed. The system can then be considered a *collisionless* system, in which a star move under a mean potential generated by all the other stars. The dSphs around the Milky Way are young enough to be collisionless. In an old or high number density galaxy, as the Milky Way itself, the stars have been perturbed so many times that they do not follow the large-scale gradient, and are not to be considered collisionless.

The luminous density for the stars in a galaxy can as a basic model be given by

$$\nu_\star(r) = \rho_\star \left(\frac{r}{r_\star}\right)^{-\gamma} \left(1 + \left(\frac{r}{r_\star}\right)^{\alpha}\right)^{-\frac{\beta-\gamma}{\alpha}}, \tag{2.4}$$

where r is the radius, $\rho_\star$ and $r_\star$ are galaxy scale parameters and α, β and γ depends on the chosen density profile. This is a very commonly used expression in dark matter research. The most common profiles are the Plummer $(\alpha, \beta, \gamma) = (2, 5, 0)$, Plummer-like $(2, 5, 0.1)$ and the non-Plummer $(2, 5, 1)$. These profiles are obtained by an Abel transform (see eq. (3.52) and (3.53)) of eq. (2.4) [9].

The analogous expression for the dark matter density ρ_{DM} (also from [9]) is

$$\rho_{\mathrm{DM}}(r) = \rho_0 \left(\frac{r}{r_0}\right)^{-\gamma'} \left(1 + \left(\frac{r}{r_0}\right)^{\alpha'}\right)^{-\frac{\beta'-\gamma'}{\alpha'}}. \tag{2.5}$$

The dark matter density profile can either be cuspy $(\alpha', \beta', \gamma') = (1, 3, 1)$ or cored $(1, 3, 0)$, where a cuspy profile diverge near the galactic center and the cored flattens out.

3

Theory

The first part of this chapter contains the definition of the J_ℓ-factor, together with a presentation of the necessary quantities for the calculation of J_ℓ. The next part will describe the underlying theory required to connect the J_ℓ to an observable. More specifically, the relation between the dark matter density and the velocity dispersion of the stars in a galaxy is derived. Finally, derivations and calculations of $F(\mathbf{v})$ and $S(v)$ will be presented to fully understand the framework.

3.1 Constituents of the J-factor

As presented in the end of the introduction, the J-factor for a dSph with self-interacting dark matter will look like eq. (2.1). In this study, the Schrödinger equation with a Yukawa potential will be solved for angular momentum quantum number $l = 0$, and thus we consider J_s:

$$J_s = \int_{\Delta\Omega} \int_{\text{l.o.s.}} \rho_{\text{DM}}^2 \langle S(v) \rangle \, \mathrm{d}s \, \mathrm{d}\Omega. \tag{3.1}$$

Here, ρ_{DM} is the dark matter mass distribution and $S(v)$ is the Sommerfeld enhancement factor. The factor $\langle S(v) \rangle$ can be expressed as $\int F(\mathbf{v})\, S(v) \mathrm{d}^3\mathbf{v}$, with $F(\mathbf{v})$ as the dark matter velocity distribution;

$$J_s = \int_{\Delta\Omega} \int_{\text{l.o.s.}} \rho_{\text{DM}}^2 \int F(\mathbf{v})\, S(\mathrm{v})\, \mathrm{d}^3\mathbf{v}\, \mathrm{d}s\, \mathrm{d}\Omega \tag{3.2}$$

To be able to calculate J_s, models of the components ρ_{DM}, $F(\mathbf{v})$ and $S(v)$ are required.

The Sommerfeld enhancement factor, $S(v)$, is based on particle physics and will be approached theoretically. More specifically, a derivation of $S(v)$ under the assumption of a Yukawa potential in the Schrödinger equation describing the annihilation will be done in section 3.5.

The determination of $F(\mathbf{v})$ is an astrophysical problem. For a galaxy which is spherically symmetric with respect to its gravitational potential and isotropic with respect to its velocity distribution, $F(\mathbf{v})$ can be uniquely determined from ρ_{DM} [18].

In this study we will perform the calculations on the dSphs based on these two assumptions. The problem of determining $F(\mathbf{v})$ is therefore reduced to deriving the relation between ρ_{DM} and $F(\mathbf{v})$. This is shown in section 3.4.

The remaining problem is to determine ρ_{DM}, the dark matter mass distribution. It can not be observed directly. Instead, a theoretical connection must be established between ρ_{DM} and some directly observable quantity. In this thesis we have chosen the velocity dispersion of the stars in the dSph. This theoretical connection will be derived in the following two sections, 3.2 and 3.3. The result is seen in the method section 4.3 in eq. (4.12).

3.2 Relation to observable data

In a spectrum from a galaxy far away one actually sees the superposition of many stellar spectra, with a Doppler shift depending on the stars' motion. This is because the galaxy is seen as just a disc and not a 3-dimensional object. By integrating the spectrum of the whole galaxy one gets a spectrum with broader absorption lines as a result of the motions of the stars. From this the velocity dispersion of the stars, $\sigma_{\text{l.o.s.}}$ is determined.

The velocity dispersion along the line of sight, $\sigma^2_{\text{l.o.s.}}$, is given by

$$\sigma^2_{\text{l.o.s.}} = \frac{1}{N}\sum_{j=1}^{N}(v_j^{\text{l.o.s.}} - v^{\text{l.o.s.}})^2, \tag{3.3}$$

where $v_j^{\text{l.o.s.}}$ is the l.o.s velocity for star j and N is the number of stars in a cylinder of volume $\mathrm{d}A \cdot \mathrm{d}l$. The latter can be calculated by integrating over the spatial density, $\nu(r)$;

$$\mathrm{d}N = \mathrm{d}A \int_{\Delta l} \mathrm{d}l\, \nu(r). \tag{3.4}$$

The integration variables $\mathrm{d}A$ and $\mathrm{d}l$ can be visualised as an infinitesimal cylinder along the line of sight in fig. 3.1. The following change of variable can be explained by the figure: $\mathrm{d}r = \mathrm{d}l\, \cos\alpha$, where $\cos\alpha = \frac{\sqrt{r^2-R^2}}{r}$. The limits comes from an integration from 0 to ∞ with the approximation of the galaxy being infinitely far away from the observer. This is then equivalent to an integration from R to ∞ multiplied by 2 and results in the following expression;

$$\mathrm{d}N = \mathrm{d}A\, 2 \int_R^\infty dr \frac{r}{\sqrt{r^2 - R^2}}\, \nu(r). \tag{3.5}$$

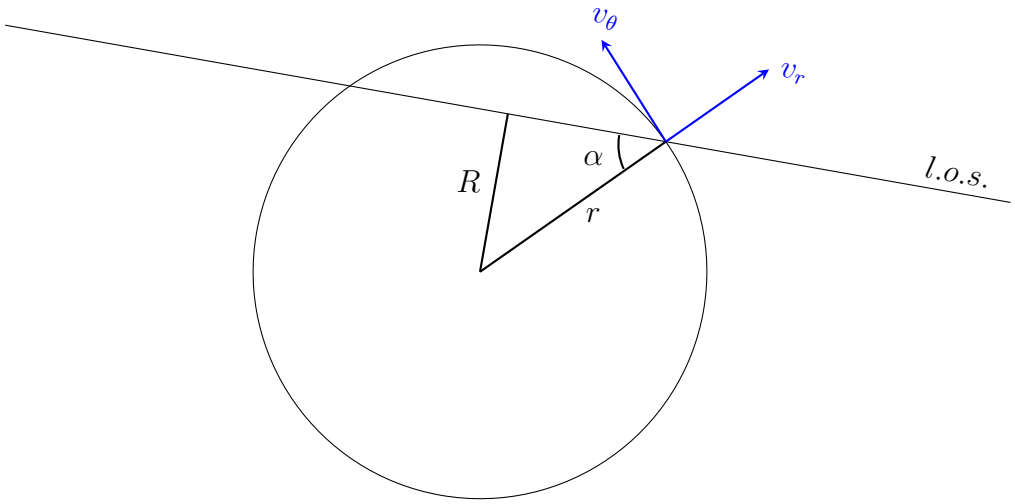

Figure 3.1: A model where the circle represents the galaxy, l.o.s. is the line of sight, r is the galaxy's radius, α is the angle between the radius and the l.o.s. and R is the orthogonal distance from the centre of the galaxy to the l.o.s. v_r and v_θ are the radial and angular velocities.

It is not possible to measure $\nu(r)$, but the luminosity density $\nu_*(r)$ is an observable. Therefore, the surface brightness $I(R)$ id defined as $\frac{N}{\mathrm{d}A}$ [18]. $I(R)$ is then

$$I(R) = 2\int_R^\infty dr \frac{r}{\sqrt{r^2 - R^2}} \nu_*(r). \tag{3.6}$$

$v^{\text{l.o.s.}}$ in eq.(3.3) is defined by

$$v^{\text{l.o.s.}} = \frac{1}{N}\sum_{j=1}^{N} v_j^{\text{l.o.s.}}. \tag{3.7}$$

In this expression $v_j^{\text{l.o.s.}}$ for a single star can not be predicted, but one can predict an average over the entire sample of stars, $\langle v_j^{l.o.s.}\rangle$. This quantity can, with help from fig. 3.1, be written as $\langle v_j^{l.o.s.}\rangle = \langle v_r\rangle \cos\alpha - \langle v_\theta\rangle \sin\alpha$, where v_r and v_θ are the radial and angular velocities respectively. Making the approximation of a static galaxy gives that $\langle v_r\rangle$ and $\langle v_\theta\rangle$ are both zero. This makes $v^{l.o.s.}$ approximately zero. In eq. (3.3) only the term $(v_j^{\text{l.o.s.}})^2$ remains in the sum for $\sigma^2_{\text{l.o.s.}}$. With $\langle v_r v_\theta\rangle = 0$ due to the spherical symmetry this gives

$$(v_j^{\text{l.o.s.}})^2 \approx \langle (v_j^{l.o.s.})^2\rangle = \langle v_r^2\rangle \cos^2\alpha - \langle v_\theta^2\rangle \sin^2\alpha. \tag{3.8}$$

Again from fig. 3.1, $\cos^2\alpha = \frac{r^2-R^2}{r^2}$ and $\sin^2\alpha = \frac{R^2}{r^2}$. Putting this in the above equation and simplifying by introducing $\beta = 1 - \langle v_\theta^2\rangle/\langle v_r^2\rangle$ gives

$$\langle (v_j^{\text{l.o.s.}})^2\rangle = \langle v_r^2\rangle \left(1 - \frac{R^2}{r^2}\beta(r)\right). \tag{3.9}$$

β is a velocity anisotropy parameter for the galaxy that describes the relation between the radial and tangential velocity dispersions, see eq. (3.33). Summation of $\langle (v_j^{\text{l.o.s.}})^2 \rangle$ over the stars j in the differential volume $\mathrm{d}A\mathrm{d}l$ yields

$$\sum_j \langle (v_j^{l.o.s.})^2 \rangle = \mathrm{d}A\, \mathrm{d}l\, \nu_*(r)\, \langle v_r^2 \rangle \left(1 - \frac{R^2}{r^2}\beta(r)\right). \tag{3.10}$$

Dividing by $I(R)$, integrating along the l.o.s. and with the same change of variable as in eq.(3.5), results in

$$\sigma^2_{\text{l.o.s.}} = \frac{2}{I(R)} \int_R^\infty \mathrm{d}r\ \nu_\star(r)\, \langle v_r^2 \rangle \left(1 - \frac{R^2}{r^2}\beta(r)\right) \frac{r}{\sqrt{r^2 - R^2}}. \tag{3.11}$$

The quantity $\nu_*(r)\, \langle v_r^2 \rangle$ is obtained in section 3.3 through Jeans equations.

3.3 Jeans equations

This section is dedicated to derive the theoretical connection between the average radial velocity of stars squared, $\langle v_r^2 \rangle$, and the density of a galaxy. This leads to a relation between our line-of-sight velocity dispersion data and the dark matter density, if one assumes that most of the galaxy's mass consist of DM.

3.3.1 Collisionless Boltzmann Equation

Given the assumptions made above, one can describe a galaxy by the collisionless Boltzmann equation. This can be shown by a simple line of reasoning, as follows.

Consider a galaxy young enough to be considered collisionless with a distribution function (DF) $f(\mathbf{x}, \mathbf{v}, t)$. Now, we can describe the coordinates by a 6-dimensional vector in phase-space, so that

$$(\mathbf{x}, \mathbf{v}) = \mathbf{w} \equiv (w_1, ..., w_6). \tag{3.12}$$

As stars move inside the galaxy, the points in phase-space changes. If the stars in the galaxy experience a smooth gravitational potential, $\Phi(\mathbf{x}, t)$ the velocity of the flow of coordinates is

$$\dot{\mathbf{w}} = (\dot{\mathbf{x}}, \dot{\mathbf{v}}) = (\mathbf{v}, -\boldsymbol{\nabla}_{\mathbf{x}}\Phi). \tag{3.13}$$

Given knowledge of $\mathbf{w}$ for every star in the galaxy at some initial time, say t_0, would by Newtons laws allow us to extract $\mathbf{w}$ at any later time t. Since the stars move smoothly through the galaxy, the flow $\dot{\mathbf{w}}$ satisfies the continuity equation, with the density $f(\mathbf{w}, t)$, given by

$$\int_V \frac{\partial f(\mathbf{w}, t)}{\partial t} \mathrm{d}^3\mathbf{x} = -\int_{\partial V} f(\mathbf{w}, t) \dot{\mathbf{w}} \cdot \mathrm{d}^2\mathbf{S}. \tag{3.14}$$

In the rest of this section we will omit the arguments of f. Now, using the divergence theorem on the right hand side and moving it to the left hand side yields

$$\int_V \left[\frac{\partial f}{\partial t} + \boldsymbol{\nabla}_{\mathbf{w}} \cdot f\dot{\mathbf{w}} \right] \mathrm{d}^3\mathbf{x} = 0. \tag{3.15}$$

Note that the divergence operator is now acting in all 6 phase-space coordinates. Since this must hold for all volumes, we can remove the integral. Expanding the divergence operator gives

$$\frac{\partial f}{\partial t} + f \underbrace{\boldsymbol{\nabla}_{\mathbf{w}} \cdot \dot{\mathbf{w}}}_{=0} + \dot{\mathbf{w}} \cdot \boldsymbol{\nabla}_{\mathbf{w}} f = 0 \tag{3.16}$$

The property that $\boldsymbol{\nabla}_{\mathbf{w}} \cdot \dot{\mathbf{w}} = 0$ follows from v_i and x_i being independent phase-space variables and that the force, $-\boldsymbol{\nabla}_{\mathbf{x}}\Phi$, is velocity independent so that

$$\begin{aligned} \frac{\partial v_i}{\partial x_i} &= 0 \\ \frac{\partial \dot{v}_i}{\partial v_i} &= \frac{\partial}{\partial v_i}(-\boldsymbol{\nabla}_{\mathbf{x}}\Phi) = 0 \end{aligned} \tag{3.17}$$

and we arrive at the collisionless Boltzmann equation

$$\frac{\partial f}{\partial t} + \dot{\mathbf{w}} \cdot \boldsymbol{\nabla}_{\mathbf{w}} f = 0. \tag{3.18}$$

In Cartesian coordinates, this is

$$\frac{\partial f}{\partial t} + \mathbf{v} \cdot \boldsymbol{\nabla}_{\mathbf{x}} f - \boldsymbol{\nabla}_{\mathbf{x}}\Phi \cdot \frac{\partial f}{\partial \mathbf{v}} = 0. \tag{3.19}$$

3.3.2 The Jeans equations

Solving the collisionless Boltzmann equation is extremely hard, as f is a function of seven variables. One can however extract valuable information regarding the solution, by taking moments of the equation. This will lead to Jeans equations, which provide an important connection between the mean radial velocity squared and the mass of the galaxy.

First, we define the spatial density, ν, and the mean velocity, $\langle \mathbf{v} \rangle = (\langle v_1 \rangle, \langle v_2 \rangle, \langle v_3 \rangle)$, of the stars as

$$\begin{aligned} \nu &\equiv \int f \, \mathrm{d}^3\mathbf{v} \\ \langle v_i \rangle &\equiv \frac{1}{\nu} \int f v_i \, \mathrm{d}^3\mathbf{v}. \end{aligned} \tag{3.20}$$

We can now study the zeroth moment of equation (3.19) by integrating over all velocities. Adopting the summation convention and writing the equation component wise then yields

$$\int \frac{\partial f}{\partial t} \mathrm{d}^3\mathbf{v} + \int v_i \frac{\partial f}{\partial x_i} \mathrm{d}^3\mathbf{v} - \int \frac{\partial \Phi}{\partial x_i} \frac{\partial f}{\partial v_i} \mathrm{d}^3\mathbf{v} = 0. \tag{3.21}$$

From the first two terms, we can take the time derivative and the spatial derivatives outside the integrals, as they do not depend on velocity. The third term vanishes, by application of the divergence theorem and knowing that no stars move infinitely fast, that is $f \to 0$ as $|\mathbf{v}| \to \infty$. We thus arrive at

$$\begin{aligned} \frac{\partial}{\partial t} \underbrace{\int f \, \mathrm{d}^3\mathbf{v}}_{=\nu} + \frac{\partial}{\partial x_i} \underbrace{\int v_i f \, \mathrm{d}^3\mathbf{v}}_{=\nu\langle v_i \rangle} - \frac{\partial \Phi}{\partial x_i} \underbrace{\int_{|\mathbf{v}|=\infty} f \, \mathrm{d}^2\mathbf{v}}_{=0} = 0 \\ \iff \frac{\partial \nu}{\partial t} + \frac{\partial (\nu \langle v_i \rangle)}{\partial x_i} = 0 \end{aligned} \tag{3.22}$$

This is a continuity equation in ν and more commonly known as the **first Jean equation**.

We proceed our analysis by taking the first moment of equation (3.19), which is done by multiplying with v_j and integrating over all velocities.

$$\int v_j \frac{\partial f}{\partial t} \, \mathrm{d}^3\mathbf{v} + \int v_j v_i \frac{\partial f}{\partial x_i} \, \mathrm{d}^3\mathbf{v} - \int v_j \frac{\partial \Phi}{\partial x_i} \frac{\partial f}{\partial v_i} \, \mathrm{d}^3\mathbf{v} = 0. \tag{3.23}$$

Again, we can take time and spatial derivatives outside the integrals, as well as the gravitational potential Φ. The equation simplifies to

$$\frac{\partial}{\partial t} \nu \langle v_j \rangle + \frac{\partial}{\partial x_i} \nu \langle v_j v_i \rangle - \frac{\partial \Phi}{\partial x_i} \int v_j \frac{\partial f}{\partial v_i} = 0 \tag{3.24}$$

where we have defined

$$\langle v_j v_i \rangle = \frac{1}{\nu} \int v_j v_i f \, \mathrm{d}^3\mathbf{v}. \tag{3.25}$$

The third term of equation (3.24) can be simplified, integrating once by parts, in the following fashion

$$\frac{\partial \Phi}{\partial x_i} \int v_j \frac{\partial f}{\partial v_i} = \frac{\partial \Phi}{\partial x_i} \int \frac{\partial v_j}{\partial v_i} f \, \mathrm{d}^3\mathbf{v} = \frac{\partial \Phi}{\partial x_i} \delta_{ji} \nu = \nu \frac{\partial \Phi}{\partial x_j} \tag{3.26}$$

and we arrive at

$$\frac{\partial}{\partial t} \nu \langle v_j \rangle + \frac{\partial}{\partial x_i} \nu \langle v_j v_i \rangle - \nu \frac{\partial \Phi}{\partial x_j} = 0 \tag{3.27}$$

which is the **second Jean equation**. Now, define the velocity dispersion tensor $\sigma_{ij}^2 = \langle v_i v_j \rangle - \langle v_i \rangle \langle v_j \rangle$, expand the first and second term in equation (3.27) by the product rule and subtract by equation (3.22) multiplied by $\langle v_j \rangle$. This yields

$$\begin{aligned}&\nu\frac{\partial\langle v_j\rangle}{\partial t} + \cancel{\langle v_j\rangle\frac{\partial\nu}{\partial t}} + \frac{\partial}{\partial x_i}\left(\nu\sigma_{ij}^2\right) + \cancel{\langle v_j\rangle\frac{\partial\nu\langle v_i\rangle}{\partial x_i}} + \nu\langle v_i\rangle\frac{\partial\langle v_j\rangle}{\partial x_i} - \nu\frac{\partial\Phi}{\partial x_j}\\ &\cancel{-\langle v_j\rangle\frac{\partial\nu}{\partial t}} - \cancel{\langle v_j\rangle\frac{\partial\nu\langle v_i\rangle}{\partial x_i}} = 0.\end{aligned} \tag{3.28}$$

Rearranging the terms gives the final result

$$\nu\frac{\partial\langle v_j\rangle}{\partial t} + \nu\langle v_i\rangle\frac{\partial\langle v_j\rangle}{\partial x_i} = -\nu\frac{\partial\Phi}{\partial x_j} - \frac{\partial}{\partial x_i}\left(\nu\sigma_{ij}^2\right) \tag{3.29}$$

known as the **third Jean equation**.

3.3.3 Spherical case

While there exists a general set of Jeans equations in spherical coordinates, we will not go through those derivations. Instead, we will make assumptions relevant for the dSphs we will look at, in order to extract the expression for $\langle v_r^2\rangle$.

First of all, we consider only stationary galaxies. This implies that all derivatives with respect to time is zero and that $\langle v_r\rangle = 0$; if the radial velocities do not cancel in mean value, our galaxy would be expanding or shrinking. Furthermore, we assume spherical symmetry. This leads to a gravitational potential only dependent on the radius, r, and that $\langle v_\theta\rangle = \langle v_\phi\rangle = 0$.

With the assumptions above, the left hand side of equation (3.29) vanishes. Furthermore, we get

$$-\nu\frac{\partial\Phi}{\partial x_j} = -\nu\frac{\partial\Phi}{\partial r}\hat{\mathbf{r}} = -\nu\frac{GM(r)}{r^2}\hat{\mathbf{r}} \tag{3.30}$$

where G is Newton's gravitational constant and $M(r) = \int_0^r \rho(s)\,\mathrm{d}s$ is the enclosed galaxy mass at radius r for a spatial density $\rho(s)$. We note here that for dSphs, the dark matter density is much larger than the density of ordinary matter, and thereof $\rho(s)$ can be replaced by the dark matter density, ρ_{DM}. Thus, this expression yields the desired connection to ρ_{DM}. Now, equation (3.29) simplifies to

$$\frac{\partial}{\partial x_i}\left(\nu\sigma_{ij}^2\right) = -\nu\frac{GM(r)}{r^2}\hat{\mathbf{r}} \tag{3.31}$$

The left hand side of this equation is a tensor divergence term. In it most general form, this a tedious expression i spherical coordinates. But as can be seen in equation (3.30) we are only interested in the radial component of this expression. Furthermore, due to the spherical symmetry all mixed terms in the velocity dispersion tensor are zero. This simplifies the spherical tensor divergence to

$$\frac{\partial\nu\sigma_{rr}^2}{\partial r} + 2\frac{\nu\sigma_{rr}^2}{r} - \frac{1}{r}(\nu\sigma_{\theta\theta}^2 + \nu\sigma_{\phi\phi}^2) = -\nu\frac{GM(r)}{r^2}. \tag{3.32}$$

Since $\sigma_{ii}^2 = \langle v_i^2 \rangle$ we get a differential equation in $\nu\langle v_r^2 \rangle$

$$\begin{aligned} &\frac{\partial \nu \langle v_r^2 \rangle}{\partial r} + 2\beta \frac{\nu \langle v_r^2 \rangle}{r} = -\nu \frac{GM(r)}{r^2}, \\ &\beta \equiv 1 - \frac{\langle v_\theta^2 \rangle + \langle v_\phi^2 \rangle}{2\langle v_r^2 \rangle} \end{aligned} \tag{3.33}$$

where β is a velocity anisotropy parameter for the galaxy. While the general solution to equation (3.33) is straightforward, we are only concerned with galaxies assumed to be isotropic, i.e. $\langle v_\theta^2 \rangle = \langle v_\phi^2 \rangle$. Consequently, $\beta = 0$ and the solution to the differential equation in this case is

$$\nu \langle v_r^2 \rangle(r) = -\int \frac{\nu(r) GM(r)}{r^2} \, \mathrm{d}r + C. \tag{3.34}$$

To obtain the solution as a definite integral, we note that the quantity $\nu\langle v_r^2 \rangle \to 0$ as $r \to \infty$ and thus we can set $C = 0$ and write the solution as

$$\nu \langle v_r^2 \rangle(r) = \int_r^\infty \frac{\nu(s) GM(s)}{s^2} \, \mathrm{d}s \,. \tag{3.35}$$

As mentioned in section 3.2 the spatial density ν is not an observable, but the luminosity density $\nu_\star$ is. With them being proportional, and the relation hidden in the luminosity profile (eq. (2.4)), eq. (3.35) becomes

$$\nu_\star \langle v_r^2 \rangle(r) = \int_r^\infty \frac{\nu_\star(s) GM(s)}{s^2} \, \mathrm{d}s \,. \tag{3.36}$$

3.4 Dark matter relative velocity distribution

By regarding two particles at a time in the annihilation process it is possible to use the reference frame for one of them. In this section we will expand this argument and develop an expression for the relative velocity distribution, in terms of the mass distribution using Eddington's inversion formula.

3.4.1 Relative velocity distribution

As we will argue in 3.5 only two particles will be taken into account during the annihilation. The probability for an annihilation of two particles will depend on both their velocities, due to that the velocities are used in the Sommerfeld enhancement. Therefore the annihilation rate will be proportional to both particles velocity distributions as described in

$$J_s \propto \int \mathrm{d}^3\mathbf{v}_1 \mathrm{d}^3\mathbf{v}_2 F_{\mathbf{x}}(\mathbf{v}_1) F_{\mathbf{x}}(\mathbf{v}_2) S(v). \tag{3.37}$$

$S(v)$ is the Sommerfeld enhancement which is discussed below, in section 3.5, and $F_{\mathbf{x}}(\mathbf{v})$ is the velocity distribution of one particle at position $\mathbf{x}$.

By using the relative velocity in the center of mass frame one can simplify the expression. The probability of the particles having center of mass velocity $\mathbf{v}_{\rm cm} = (\mathbf{v}_1 + \mathbf{v}_2)/2$ and relative velocity $\mathbf{v}_{\rm rel} = \mathbf{v}_1 - \mathbf{v}_2$ must be equal to the probability of them having velocities $\mathbf{v}_1$ and $\mathbf{v}_2$. Noting that $\mathrm{d}^3\mathbf{v}_1\mathrm{d}^3\mathbf{v}_2 = \mathrm{d}^3\mathbf{v}_{\rm cm}\mathrm{d}^3\mathbf{v}_{\rm rel}$, the change of variables give

$$F_{\mathbf{x}}(\mathbf{v}_1)F_{\mathbf{x}}(\mathbf{v}_2)\mathrm{d}^3\mathbf{v}_1\mathrm{d}^3\mathbf{v}_2 = F_{\mathbf{x}}(\mathbf{v}_{\rm cm} + \mathbf{v}_{\rm rel}/2)F_{\mathbf{x}}(\mathbf{v}_{\rm cm} - \mathbf{v}_{\rm rel}/2)\mathrm{d}^3\mathbf{v}_{\rm cm}\mathrm{d}^3\mathbf{v}_{\rm rel}. \tag{3.38}$$

J_s depends only on the relative velocity, since the centre of mass velocity does not describe how the particles move closer together and annihilation is local, see below in section 3.5.2. Therefore the above expression can be integrated over $v_{\rm cm}$ to obtain the relative velocity distribution,

$$F_{\mathbf{x},\rm rel}(\mathbf{v}_{\rm rel})\,\mathrm{d}^3\mathbf{v}_{\rm rel} = \int F_{\mathbf{x}}(\mathbf{v}_{\rm cm} + \mathbf{v}_{\rm rel}/2)F_{\mathbf{x}}(\mathbf{v}_{\rm cm} - \mathbf{v}_{\rm rel}/2)\mathrm{d}^3\mathbf{v}_{\rm cm}\,\mathrm{d}^3\mathbf{v}_{\rm rel}. \tag{3.39}$$

To make further simplifications the properties of the distribution $F_{\mathbf{x}}(\mathbf{v})$ need to be developed.

At a point $\mathbf{x}$ in the halo the dark matter velocity distribution, $F_{\mathbf{x}}(\mathbf{v})$, can by definition be written as

$$F_x(\mathbf{v})\mathrm{d}^3\mathbf{v} \equiv \frac{f(\mathbf{x},\mathbf{v})}{\rho(\mathbf{x})}\,\mathrm{d}^3\mathbf{v}, \tag{3.40}$$

where $f(\mathbf{x},\mathbf{v})$ is the phase-space density and $\rho(\mathbf{x})$ is the dark matter mass distribution, which can be defined as $\rho(\mathbf{x}) \equiv \int f(\mathbf{x},\mathbf{v})\mathrm{d}^3\mathbf{v}$ [16]. We make the assumptions that the mass distribution is spherically symmetric, i.e. $\rho(\mathbf{x}) = \rho(r)$, and that the velocity is isotropic. As a result the phase space density only depends on the radii, r, and the magnitude of the velocity, $f(\mathbf{x},\mathbf{v}) = f(r,v)$. Therefore the the velocity distribution is independent of direction, i.e. $F_{\mathbf{x}}(\mathbf{v})\mathrm{d}^3\mathbf{v} = F_r(v)\,\mathrm{d}v$ and the two directions can be integrated out:

$$F_r(v)\,\mathrm{d}v = 4\pi v^2\frac{f(r,v)}{\rho(r)}\,\mathrm{d}v\,. \tag{3.41}$$

With this we can rewrite equation (3.39) as

$$F_r(v_{\rm rel})\,\mathrm{d}v_{\rm rel} = 4\pi v_{\rm rel}^2\int\frac{f(r,|\mathbf{v}_{\rm cm} + \mathbf{v}_{\rm rel}/2|)f(r,|\mathbf{v}_{\rm cm} - \mathbf{v}_{\rm rel}/2|)}{\rho^2(r)}\,\mathrm{d}^3\mathbf{v}_{\rm cm}\mathrm{d}v_{\rm rel}. \tag{3.42}$$

The argument $|\mathbf{v}_{\rm cm} \pm \mathbf{v}_{\rm rel}/2|$ is independent of one angle, thus 2π can be integrated out. The other angle is between $\mathbf{v}_{\rm cm}$ and $v_{\rm rel}$ and therefore $|\mathbf{v}_{\rm cm} \pm \mathbf{v}_{\rm rel}/2| = v_{\rm cm}z \pm v_{\rm rel}/2$, $z \in [-1,1]$. Then the relative velocity distribution is

$$F_r(v_{\rm rel})\,\mathrm{d}v_{\rm rel} = 8\pi^2 v_{\rm rel}^2\int_0^\infty v_{\rm cm}^2\int_{-1}^1\frac{f(r,v_{\rm cm}z + v_{\rm rel}/2)f(r,v_{\rm cm}z - v_{\rm rel}/2)}{\rho^2(r)}\,\mathrm{d}z\,\mathrm{d}v_{\rm cm}\,\mathrm{d}v_{\rm rel}, \tag{3.43}$$

where the subscript r in $F_r(v_{\rm rel})$ indicates that this velocity distribution is for one specific radii. f is the phase space distribution and ρ is the mass distribution.

3.4.2 Application of Jeans theorem

As mentioned above (section 3.3.2) the collisionless Boltzmann equation almost impossible to solve, since it is a function of seven variables. To obtain exact solutions one can regard only a subset of all possible stellar dynamical equilibria at a time. This will be done for steady-state dSphs, in order to obtain Eddington's formula in the next section.

We base the derivation on the Jeans theorem (Binney and Tremaine, p. 200, [18]):

Any steady-state solution to the collisionless Boltzmann equation depends on the phase-space coordinates only through integrals of motion in the galactic potential, and any function of the integrals yields a steady-state solution of the collisionless Boltzmann equation.

Assuming a steady-state spherically symmetric system, the distribution function (DF) is a function of the energy, E, and the angular momentum, $\mathbf{L}$. E is an integral of motion in any static potential and $\mathbf{L}$ is in an spherical potential constituted by three integrals of motion. An integral of motion is any function of $(\mathbf{x}, \mathbf{v})$ that is constant along any orbit. By the Jeans theorem, any non-negative function of the mentioned integrals can be the DF of a spherical stellar system. Due to the spherical symmetry the function will only depend on the magnitude of $\mathbf{L}$. With f as the DF, and for a stellar system that itself provides the potential Φ, one has

$$\nabla^2\Phi = 4\pi G\rho = 4\pi G \int f \,\mathrm{d}^3\mathbf{v}\,. \tag{3.44}$$

The same equation after exploiting spherical symmetry (Φ depends only on r) is called the fundamental equation of spherical equilibrium stellar systems, and is defined by

$$\frac{1}{r^2}\frac{\mathrm{d}}{\mathrm{d}r}\left(r^2\frac{\mathrm{d}\Phi}{\mathrm{d}r}\right) = 4\pi G \int f\left(\frac{1}{2}|\mathbf{v}|^2 + \Phi|\mathbf{r}\times\mathbf{v}|\right)\mathrm{d}^3\mathbf{v}\,. \tag{3.45}$$

To simplify future calculations, the relative potential Ψ and the relative energy $\mathcal{E}$ are defined as

$$\Psi = -\Phi + \Phi_0 \tag{3.46}$$

and

$$\mathcal{E} = -E + \Phi_0 = \Psi - \frac{1}{2}v^2, \tag{3.47}$$

with Φ_0 chosen to satisfy $f > 0$ for $\mathcal{E} > 0$ and $f = 0$ for $\mathcal{E} \leqslant 0$. The relative potential then satisfies Poisson's equation through $\nabla^2\Psi = -4\pi G\rho$, where $\Psi \to \Phi_0$ as $x \to \infty$.

For a system with isotropic velocity-dispersion tensor the DF will depend only on $\mathcal{E}$ and not L. Eq. (3.45) then becomes (in spherical coordinates)

$$\frac{1}{r^2}\frac{\mathrm{d}}{\mathrm{d}r}\left(r^2\frac{\mathrm{d}\Phi}{\mathrm{d}r}\right) = -4\pi G\int_0^{\sqrt{2\Psi}} f(\mathcal{E})4\pi v^2\mathrm{d}v = -16\pi^2 G\int_0^{\sqrt{2\Psi}} f\Big(\Psi - \frac{1}{2}v^2\Big)v^2\,\mathrm{d}v\,, \tag{3.48}$$

where the upper limit is decided by $f \neq 0$ for $\mathcal{E} = \Psi - \frac{1}{2}v^2 > 0$. A change of variable from v to $\mathcal{E}$ in eq. (3.48), with $\mathrm{d}\mathcal{E} = -v\mathrm{d}v$ and limits $v = 0 \to \mathcal{E} = \Psi$ and $v = \sqrt{2\Psi} \to \mathcal{E} = 0$, results in

$$\frac{1}{r^2}\frac{\mathrm{d}}{\mathrm{d}r}\left(r^2\frac{\mathrm{d}\Phi}{\mathrm{d}r}\right) = -16\pi^2 G\int_0^{\Psi} f(\mathcal{E})\sqrt{2(\Psi(r)-\mathcal{E})}\,\mathrm{d}\mathcal{E}. \tag{3.49}$$

3.4.3 Eddington inversion formula

With the Eddington inversion formula one can derive the DF $f(\mathcal{E})$ for any given mass density $\rho(r)$. $f(\mathcal{E})$ will then be used to compose a velocity distribution, which will take part in eq.(3.43). The theory from the former section is used.

To achieve this formula for the density, notice that Ψ is an monotonic function of r, due to the spherical symmetry, and use the same change of variable as in eq.(3.49):

$$\rho(r) = \int f\mathrm{d}^3\mathbf{v} = 4\pi\int v^2 f\Big(\Psi - \frac{1}{2}v^2\Big)\mathrm{d}v = 4\pi\int_0^{\Psi} f(\mathcal{E})\sqrt{2(\Psi(r)-\mathcal{E})}\mathrm{d}\mathcal{E} \tag{3.50}$$

The above equation is then differentiated with respect to Ψ, resulting in

$$\frac{1}{\sqrt{8}\pi}\frac{\mathrm{d}\rho}{\mathrm{d}\Psi} = \int_0^{\Psi}\frac{f(\mathcal{E})}{\sqrt{\Psi(r)-\mathcal{E}}}\mathrm{d}\mathcal{E}. \tag{3.51}$$

This is an Abel integral on the form

$$f(x) = \int_0^x \frac{g(t)\mathrm{d}t}{(x-t)^{\alpha}}, \quad 0 < \alpha < 1 \tag{3.52}$$

which has the solution [18]

$$g(t) = \frac{\sin(\pi\alpha)}{\pi}\int_0^t \frac{f(x)\mathrm{d}x}{(t-x)^{1-\alpha}}. \tag{3.53}$$

The above formula for solving the Abel integral gives the following solution to eq.(3.51)

$$f(\mathcal{E}) = \frac{1}{\sqrt{8}\pi^2}\frac{\mathrm{d}}{\mathrm{d}\mathcal{E}}\int_0^{\mathcal{E}}\frac{\mathrm{d}\Psi}{\sqrt{\mathcal{E}-\Psi(r)}}\frac{\mathrm{d}\rho}{\mathrm{d}\Psi}. \tag{3.54}$$

Since $f(\mathcal{E}) \geqslant 0$ everywhere, the function $\int_0^{\mathcal{E}}\frac{d\Psi}{\sqrt{\mathcal{E}-\Psi(r)}}$ has to be an increasing function of $\mathcal{E}$. Otherwise, the solution is unphysical. Applying Leibniz integral rule on eq.(3.54) gives the alternative form, which is called Eddington's formula;

$$f(\mathcal{E}) = \frac{1}{\sqrt{8}\pi^2}\left[\int_0^{\mathcal{E}}\frac{d\Psi}{\sqrt{\mathcal{E}-\Psi(r)}}\frac{d^2\rho}{d\Psi^2} + \frac{1}{\sqrt{\mathcal{E}}}\Big(\frac{d\rho}{d\Psi}\Big)_{\Psi=0}\right]. \tag{3.55}$$

This expression is rewritten with help from the chain rule, since ρ is not usually given as a function of Ψ:

$$\frac{\mathrm{d}^2\rho}{\mathrm{d}\Psi^2} = \left(\frac{\mathrm{d}\Psi}{\mathrm{d}r}\right)^{-2}\frac{\mathrm{d}^2\rho}{\mathrm{d}r^2} + \frac{\mathrm{d}^2r}{\mathrm{d}\Psi^2}\frac{\mathrm{d}\rho}{\mathrm{d}r} \quad \text{and} \quad \frac{\mathrm{d}^2r}{\mathrm{d}\Psi^2} = -\frac{\mathrm{d}^2\Psi}{\mathrm{d}r^2}\left(\frac{\mathrm{d}\Psi}{\mathrm{d}r}\right)^{-3} \tag{3.56}$$

gives

$$\frac{\mathrm{d}^2\rho}{\mathrm{d}\Psi^2} = \left(\frac{\mathrm{d}\Psi}{\mathrm{d}r}\right)^{-2}\left(\frac{\mathrm{d}^2\rho}{\mathrm{d}r^2} - \left(\frac{\mathrm{d}\Psi}{\mathrm{d}r}\right)^{-1}\frac{\mathrm{d}^2\Psi}{\mathrm{d}r^2}\frac{\mathrm{d}\rho}{\mathrm{d}r}\right). \tag{3.57}$$

From a numerical point of view it is easier to change the variable to the radius of the spherical system, r, according to $\mathrm{d}\Psi = \frac{\mathrm{d}\Psi}{\mathrm{d}r}\mathrm{d}r$. Assuming only dark matter contributes to the gravitational potential and the density, eq. (3.55) becomes

$$\begin{aligned} f(\mathcal{E}) = {} & \frac{1}{\sqrt{8}\pi^2}\int_{\Psi_{DM}^{-1}(\mathcal{E})}^{\infty}\frac{1}{\sqrt{\mathcal{E}-\Psi_{DM}(r)}}\times \\ & \left[\frac{d\rho_{DM}}{dr}\frac{d^2\Psi_{DM}}{dr^2}\left(\frac{d\Psi_{DM}}{dr}\right)^{-2} - \frac{d^2\rho_{DM}}{dr^2}\left(\frac{d\Psi_{DM}}{dr}\right)^{-1}\right]dr. \end{aligned} \tag{3.58}$$

From this DF $f(\mathcal{E})$ one can reach a velocity distribution by making use of the relation in eq. (3.47), namely $\mathcal{E} = \Psi(r) - \frac{1}{2}v^2$. $f(\mathcal{E})$ then becomes $f(\Psi(r) - \frac{1}{2}v^2)$. This $f(\Psi(r) - \frac{1}{2}v^2)$ is identified as the $f(r, v)$ from eq.(3.43) in section 3.4.1, with $v = v_{\mathrm{cm}}z \pm v_{\mathrm{rel}}/2$, namely

$$\begin{aligned} F_r(v_{\mathrm{rel}})\,\mathrm{d}v_{\mathrm{rel}} = {} & 8\pi^2 v_{\mathrm{rel}}^2\times \\ & \int_0^{\infty} v_{\mathrm{cm}}^2\int_{-1}^{1}\frac{f(r, v_{\mathrm{cm}}z + v_{\mathrm{rel}}/2)f(r, v_{\mathrm{cm}}z - v_{\mathrm{rel}}/2)}{\rho^2(r)_{\mathrm{DM}}}\,\mathrm{d}z\,\mathrm{d}v_{\mathrm{cm}}\,\mathrm{d}v_{\mathrm{rel}}. \end{aligned} \tag{3.59}$$

Noticing that the integrand is symmetric in z, giving a factor 2 when integrating from 0 to 1 instead, and using that $v^2 = v_{\mathrm{cm}}^2/2 + v_{\mathrm{rel}}^2/8 \pm v_{\mathrm{cm}}v_{\mathrm{rel}}z/2$, the relative velocity distribution becomes

$$\begin{aligned} F_r(v_{\mathrm{rel}})\,\mathrm{d}v_{\mathrm{rel}} = \frac{16\pi^2 v_{\mathrm{rel}}^2}{\rho_{\mathrm{DM}}^2(r)}\int_0^{\infty} v_{\mathrm{cm}}^2\int_0^1 & f\Big(\Psi(r) - \frac{v_{\mathrm{cm}}^2}{2} - \frac{v_{\mathrm{rel}}^2}{8} - \frac{v_{\mathrm{cm}}v_{\mathrm{rel}}z}{2}\Big)\times \\ & f\Big(\Psi(r) - \frac{v_{\mathrm{cm}}^2}{2} - \frac{v_{\mathrm{rel}}^2}{8} + \frac{v_{\mathrm{cm}}v_{\mathrm{rel}}z}{2}\Big)\,\mathrm{d}z\,\mathrm{d}v_{\mathrm{cm}}\,\mathrm{d}v_{\mathrm{rel}}. \end{aligned} \tag{3.60}$$

Combining these two equations gives further limitations to the integration boundaries in eq. (3.60), since $f(\mathcal{E}) = 0$ for $\mathcal{E} \leqslant 0$ (as discussed after eq. (3.47)). $\mathcal{E} \geqslant 0$ gives $\Psi(r) - \frac{1}{2}v^2 \geqslant 0 \rightarrow v^2 \leqslant 2\Psi(r)$ and the maximum $v^2 = v_{\mathrm{cm}}^2 + v_{\mathrm{rel}}^2/4 + v_{\mathrm{cm}}v_{\mathrm{rel}}z$ gives

$$2\Psi \geqslant v_{\mathrm{cm}}^2 + \frac{v_{\mathrm{rel}}^2}{4} \pm v_{\mathrm{cm}}v_{\mathrm{rel}}z \iff z \leqslant \frac{8\Psi - 4v_{\mathrm{cm}}^2 - v_{\mathrm{rel}}}{4v_{\mathrm{cm}}v_{\mathrm{rel}}}. \tag{3.61}$$

Combining $v^2 \leqslant 2\Psi(r)$ with $0 \leqslant z \leqslant 1$ results in the following inequalities, the first for $z = 1$

$$v_{\mathrm{cm}}^2 + \frac{v_{\mathrm{rel}}^2}{4} + v_{\mathrm{cm}}v_{\mathrm{rel}} = \Big(v_{\mathrm{cm}} + \frac{v_{\mathrm{rel}}}{2}\Big)^2 \leqslant 2\Psi \iff v_{\mathrm{cm}} \leqslant \sqrt{2\Psi} - \frac{v_{\mathrm{rel}}}{2} \tag{3.62}$$

and the second for $z = 0$

$$v_{\rm cm}^2 + \frac{v_{\rm rel}^2}{4} \leqslant 2\Psi \iff v_{\rm cm} \leqslant \frac{\sqrt{8\Psi - v_{\rm rel}^2}}{2}. \tag{3.63}$$

These integration limits give the final expression for relative velocity distribution:

$$F_r(v_{\rm rel})\,\mathrm{d}v_{\rm rel} = \frac{16\pi^2 v_{\rm rel}^2}{\rho^2(r)_{\rm DM}} \times \left(\int_0^{\sqrt{2\Psi} - \frac{v_{\rm rel}}{2}} v_{\rm cm}^2 \int_0^1 A\,\mathrm{d}z\,\mathrm{d}v_{\rm cm} + \int_{\sqrt{2\Psi} - \frac{v_{\rm rel}}{2}}^{\frac{\sqrt{8\Psi - v_{\rm rel}^2}}{2}} v_{\rm cm}^2 \int_0^{\frac{8\Psi - 4v_{\rm cm}^2 - v_{\rm rel}}{4 v_{\rm cm} v_{\rm rel}}} A\,\mathrm{d}z\,\mathrm{d}v_{\rm cm} \right) \tag{3.64}$$

where

$$A = f\left(\Psi(r) - \frac{v_{\rm cm}^2}{2} - \frac{v_{\rm rel}^2}{8} - \frac{v_{\rm cm} v_{\rm rel} z}{2}\right) f\left(\Psi(r) - \frac{v_{\rm cm}^2}{2} - \frac{v_{\rm rel}^2}{8} + \frac{v_{\rm cm} v_{\rm rel} z}{2}\right).$$

3.5 Sommerfeld enhancement

One of the most important physical quantities in nuclear and particle physics is the cross section. Classically, this is the area transverse to the relative motion of two particles within which a scattering process, a particle collision, can occur. However, a scattering process is intrinsically stochastic: even if the particles meet within the cross section area, the particle collision might still not occur [19]. The more rigorous formulation of the cross section therefore relies on quantum mechanics. Given a probability density current, the cross section times this equals the number of scattered particles. The cross section is thus proportional to the probability of collision between two particles. Since annihilation of two particles is nothing more than a particle collision resulting in a transformation of the particles, the importance of the cross section for an annihilation process is indisputable.

If there exists a long-range potential between the particles, the cross section will change due to some form of force between the particles. If the force is attractive the cross section will be greater and if it is repulsive it will be smaller. When a potential between the particles is accounted for it is called a Sommerfeld enhancement. It is also important to note that the Sommerfeld enhancement is usually referred to in non-relativistic quantum mechanics. The new cross section due to the potential is always proportional to the old one not accounting for the same. Thus the Sommerfeld enhancement can be expressed as a Sommerfeld enhancement factor:

$$\sigma = S(v)\sigma_0 \tag{3.65}$$

where σ_0 is the old cross section, σ the new one and S the Sommerfeld enhancement factor with a dependence on the relative velocity v. In the two next paragraphs, a description of the Yukawa potential and a derivation of the enhancement factor S follows.

3.5.1 Yukawa potential

In particle physics, a force between two particles can be described as an exchange of a force mediator particle. The properties of this exchange particle affects the properties of the force [11]. The Yukawa potential describes one such force and has the form;

$$V_{Yukawa}(r) = \alpha \frac{e^{-m_\phi r}}{r} \tag{3.66}$$

where α is the strength of the potential, r the radial coordinate and m_ϕ the mass of the mediator particle. The Coulomb potential is a special case of the Yukawa potential where the force exchange particle, the photon, has zero mass. The Yukawa potential corresponds to a long-range force which can describe the self-interaction between dark matter particles. Thus, it can lead to a Sommerfeld enhancement. Nonetheless, it is very simple in its form. It is for these reasons it has been chosen as the subject potential for this study.

3.5.2 Sommerfeld enhancement for an annihilation process

To fully derive the Sommerfeld enhancement, one must refer to quantum field theory. This is beyond the scope of this report. Instead, we will derive an expression of how an elastic scattering process is enhanced by introducing a long range potential. Then we will argue that the same result also applies to an annihilation process.

Imagine two particles, both travelling with a non-relativistic velocity and a local interaction, an interaction in a point, between the two in the form of a Hamiltonian $\hat{H}_{local}$. This two-body-system can always be simplified to a single-body-system in which one particle is seen as stationary and the other travelling with a velocity equal to the relative velocity with a mass equal to the reduced mass. We will now derive the cross section for this system. First, we will do this without any self-interaction between the particles. Then, we will do the same for a Yukawa self-interaction and compare the results to identify the Sommerfeld enhancement factor.

The total Hamiltonian of the system without self-interaction can be written as

$$\hat{H} = \hat{H}_0 + \hat{H}_{local} = \frac{\hat{p}^2}{2\mu} + \hat{H}_{local} \tag{3.67}$$

where μ is the reduced mass of the two particles. The solution of the Hamiltonian $\hat{H}_0$ is the plane-wave free particle solution, $|\phi\rangle = e^{i\mathbf{k}\cdot\mathbf{x}}$, exhibiting a continuous energy spectra for the time independent Schrödinger equation:

$$\hat{H}_0|\phi\rangle = E|\phi\rangle \tag{3.68}$$

If we assume that the scattering process preserves energy, an elastic scattering process, the same energy eigenvalues goes with $\hat{H}$. The time independent formulation of the scattering process can then be expressed as:

$$\hat{H}|\psi\rangle = (\hat{H}_0 + \hat{H}_{local})|\psi\rangle = E|\psi\rangle \tag{3.69}$$

We wish to find the solution $|\psi\rangle$ to this equation. It is apparent that as $\hat{H}_{local} \to 0$ the solution $|\psi\rangle \to |\phi\rangle$. Thus it is reasonable to expect the solution $|\psi\rangle$ to depend on $|\phi\rangle$. One can then deduce an implicit expression for the solution to (3.69):

$$|\psi\rangle = |\phi\rangle + (E - \hat{H}_0)^{-1}\hat{H}_{local}|\psi\rangle \equiv |\phi\rangle + \frac{1}{E - \hat{H}_0}\hat{H}_{local}|\psi\rangle \tag{3.70}$$

The reader can check this by applying $E - \hat{H}_0$ to (3.70), yielding equation (3.69). However, to avoid problems arising with a singular operator as $\frac{1}{E-\hat{H}_0}$, one usually makes E slightly complex, leading to the Lippman-Schwinger equation [20]:

$$|\psi^{(\pm)}\rangle = |\phi\rangle + \frac{1}{E - \hat{H}_0 \pm i\epsilon}\hat{H}_{local}|\psi^{(\pm)}\rangle \tag{3.71}$$

By multiplying with $\langle\mathbf{x}|$ from the left and using the resolution of identity; $1 = \int d^3x'\langle\mathbf{x}'|\mathbf{x}'\rangle$, one yield the implicit solution in the position basis:

$$\langle\mathbf{x}|\psi^{(\pm)}\rangle = \langle\mathbf{x}|\phi\rangle + \int d^3x'\langle\mathbf{x}|\frac{1}{E - \hat{H}_0 \pm i\epsilon}|\mathbf{x}'\rangle\langle\mathbf{x}'|\hat{H}_{local}|\psi^{(\pm)}\rangle \tag{3.72}$$

This is an integral equation, more precisely an inhomogenous Fredholm equation of the second kind. The kernel of the integral equation is:

$$K_{\pm}(x, x') \equiv \frac{\hbar^2}{2\mu}\langle\mathbf{x}|\frac{1}{E - \hat{H}_0 \pm i\epsilon}|\mathbf{x}'\rangle \tag{3.73}$$

It can be shown by using the resolution of identity again, but now in the momentum basis, and the method of residues, that

$$K_{\pm}(x, x') = -\frac{e^{\pm ik|\mathbf{x}-\mathbf{x}'|}}{4\pi|\mathbf{x} - \mathbf{x}'|} \tag{3.74}$$

if E is expressed as $\hbar^2k^2/2\mu$ where k is the modulus of the wave vector (remember that E is the same as in the case of a plane-wave). The locality of $\hat{H}_{local}$ can be expressed as:

$$\langle\mathbf{x}'|\hat{H}_{local}|\mathbf{x}''\rangle = H_{local}(\mathbf{x}')\delta^3(\mathbf{x}' - \mathbf{x}''). \tag{3.75}$$

One can also use the fact that $H_{local}(\mathbf{x}') = U_{local}\delta(\mathbf{x}')$, where U_{local} is a constant. Altogether, this yields:

$$\begin{aligned}
\langle\mathbf{x}|\psi^{(\pm)}\rangle &= \langle\mathbf{x}|\phi\rangle - \frac{\mu}{\hbar^2}\int d^3x'\frac{e^{\pm ik|\mathbf{x}-\mathbf{x}'|}}{4\pi|\mathbf{x} - \mathbf{x}'|}H_{local}(\mathbf{x}')\langle\mathbf{x}'|\psi^{(\pm)}\rangle \\
&= \langle\mathbf{x}|\phi\rangle - \underbrace{\frac{\mu U_{local}}{2\pi\hbar^2}\psi^{(\pm)}(0)}_{A}\frac{e^{\pm ik|\mathbf{x}|}}{|\mathbf{x}|} \\
&\equiv \langle\mathbf{x}|\phi\rangle - A\frac{e^{\pm ikr}}{r}.
\end{aligned} \tag{3.76}$$

Here A is an amplitude factor with a linear dependence on $\psi^{(\pm)}(0)$.

The physical interpretation of this solution can be clarified by analysing each term separately. The first term is a plane wave representing the incoming particle. The second term is a spherical wave representing the scattered end products of the annihilation, at least for the + solution. The − solution is an *incoming* spherical wave and such a system is not physically realisable in this situation.

The cross section is simply a scattering probability. Therefore, if we imagine a large number of particles prepared identically according to the described situation, the probability of finding a scattered particle going through a small area da far away from the scattering centre is:

$$d\sigma = \frac{\text{number of particles scattered into } da \text{ per unit time}}{\text{number of incident particles crossing unit area per unit time}} \tag{3.77}$$

We can relate this to the probability currents, $\mathbf{j}$, associated with the wave functions of the incoming and outgoing stream of particles respectively:

$$d\sigma = \frac{r^2 d\Omega |\mathbf{j_{scat}}|}{|\mathbf{j_{inc}}|} \tag{3.78}$$

where $d\Omega$ is the usual differential solid angle and r is the radial coordinate sufficiently far away from the scattering centre. With the interpretation of equation (3.76) one yields:

$$d\sigma = \frac{r^2 d\Omega |A\frac{e^{ikr}}{r}|^2}{|e^{i\mathbf{k}\cdot\mathbf{x}}|^2} = |A|^2 d\Omega. \tag{3.79}$$

The total cross section is the solid angle integral of this differential probability. From the definition of A, we can conclude that the cross section is always proportional to the squared modulus of the wave function at zero ; $|\psi(0)|^2$. This makes intuitive sense since the squared modulus of the wave function at zero represents the probability of finding a particle at the origin, where the local interaction takes place. As a reminder, this wavefunction is the solution to the Schrödinger equation with the Hamiltonian in equation (3.67). Since we do not know this wavefunction, the cross section is also unknown. In this situation, one usually makes the Born-approximation. That is, we assume that this wavefunction differs only little from our original plane-wave solution. One can then substitute $|\psi\rangle$ with $|\phi\rangle$ in equation (3.76) under the integral. Thus,

$$\sigma_0 \approx \int_{all\ \ solid\ \ angles} d\sigma = 4\pi \left| \frac{\mu U_{local}}{2\pi\hbar^2} \phi(0) \right|^2 \propto \left| \phi(0) \right|^2. \tag{3.80}$$

Now, if one does the same for a Yukawa self-interaction, the solution looks very much the same. The only difference is that a Yukawa potential is included in $\hat{H}_0$. As a result, the usual plane-wave solution, $\phi(0)$, is perturbed. The new cross section accounting for the Yukawa potential is thus proportional to the squared modulus of another perturbed wave function at zero. This wave function corresponds to the Schrödinger equation:

$$(\frac{\hat{\mathbf{p}}^2}{2\mu} + \hat{V}_{Yukawa})\Psi = \frac{\hbar^2 k^2}{2\mu}\Psi. \tag{3.81}$$

Thus the Sommerfeld enhancement in equation (3.65) is given by:

$$S(v) = \frac{\sigma_{Yukawa}}{\sigma_0} = \frac{|\Psi(0)|^2}{|\phi(0)|^2} = |\Psi(0)|^2 \tag{3.82}$$

where the plane-wave is again taken as normalised to 1. The determination of the Sommerfeld factor for the Yukawa potential is thus reduced to determining the modulus of the wave function in equation (3.81) at zero given the boundary condition:

$$\Psi \to e^{i\mathbf{k}\cdot\mathbf{x}} + A\frac{e^{ikr}}{r} \quad \text{as } r \to \infty. \tag{3.83}$$

This boundary condition describes a plane wave and spherical wave as r goes to infinity.

This very same result also applies for an annihilation process [21]. The difference between a scattering process and annihilation is that the latter is not an elastic process since the ingoing particles are different from the outgoing. However, the probability of annihilation is also proportional to the probability of finding the fictious particle at the origin [21]. The Sommerfeld enhancement for an annihilation process must then be precisely the squared modulus of the wave function in eq. (3.82).

3.5.3 The relation between the Sommerfeld enhancement and the radial wave function's asymptotic behaviour

The purpose of this section is to derive the explicit expression for the Sommerfeld enhancement that later will be used in this study. In short terms the derivation involves a symmetry argument, a statement that only the radial wave function is of importance, a change of variables and an analysis of the asymptotic behaviour of this radial wave function.

The Schrödinger equation in equation (3.81) with the explicit expression for the Yukawa potential is:

$$(-\frac{\hbar^2}{2\mu}\partial_{\mathbf{r}}^2 + \frac{\alpha e^{-m_\phi r}}{r})\Psi_{\mathbf{p}}(\mathbf{r}) = \frac{\mathbf{p}^2}{2\mu}\Psi_{\mathbf{p}}(\mathbf{r}) \tag{3.84}$$

where the index $\mathbf{p}$ has been introduced to illustrate the momentum dependence of the solution Ψ. Since the Yukawa potential is spherically symmetric, the solution is rotationally symmetric about the axis of propagation of the wave function. The solution can then be decomposed in partial waves [21, 22]:

$$\Psi_{\mathbf{p}}(\mathbf{r}) = \frac{(2\pi)^{3/2}}{4\pi p}\sum_{l=0}^{\infty} i^l(2l+1)e^{\delta_l}R_{p,l}(r)P_l(\cos\theta). \tag{3.85}$$

Here, P_l are the Legendre polynomials, δ_l a scattering phase shift and $R_{p,l}$ is the radial part satisfying the radial Schrödinger equation:

$$(\frac{d^2}{dr^2} + \frac{2}{r}\frac{d}{dr} - \frac{l(l+1)}{r^2} + \frac{p^2}{\hbar^2} + \frac{2\mu\alpha e^{-m_\phi r}}{\hbar^2 r})R_{p,l}(r) = 0, \tag{3.86}$$

normalised as

$$\int_0^\infty r^2 R_{p,l}(r) R_{p',l}(r) dr = \delta(p - p'), \tag{3.87}$$

with completeness relation

$$\int_0^\infty R_{p,l}(r) R_{p,l}(r') dp = \frac{1}{r^2}\delta(p - p'). \tag{3.88}$$

One can show that the resulting square of the wave function, and thus the Sommerfeld enhancement, satisfies:

$$|\Psi_{\mathbf{p}}(0)|^2 = \left|\sqrt{\frac{\pi}{2}}\frac{(2l+1)!!}{l!}\frac{1}{p}\frac{d^l}{dr^l}R_{p,l}(r)\Big|_{r=0}\right|^2 \tag{3.89}$$

This quite tedious derivation will not be included in this report (consider instead R. Iengo [21]). Thus for our purposes, the problem is reduced to determining the behaviour of the radial part $R_{p,l}(r)$ at the origin.

The normalisation in equation (3.87) corresponds to an asymptotic behaviour [22]

$$R_{p,l}(r) \to \sqrt{\frac{2}{\pi}}\frac{\sin\left(pr - \frac{l\pi}{2} + \delta_l\right)}{r} \quad \text{as } r \to \infty. \tag{3.90}$$

Let us define $pr = x$. If the radial function is expressed as

$$R_{p,l}(r) = Npx^l \Phi_l(x), \tag{3.91}$$

one finds that the differential equation in (3.86) is simplified by the loss of one term:

$$\Phi_l'' + \frac{2(l+1)}{x}\Phi_l' + (\frac{2\mu\alpha e^{-\frac{m_\phi}{p}x}}{\hbar^2 px} + \frac{1}{\hbar^2})\Phi_l = 0. \tag{3.92}$$

The corresponding asymptotic behaviour for Φ is

$$x^{l+1}\Phi_l(x) \to C\sin\left(x - \frac{l\pi}{2} + \delta_l\right) \quad \text{as } x \to \infty. \tag{3.93}$$

Comparison with equation (3.90), using equation (3.91), gives: $N = \sqrt{\frac{2}{\pi}}\frac{1}{C}$. By combining this relation and the two identities (3.89) and (3.91) one yields:

$$S(v) = \left(\frac{(2l+1)!!}{C}\right)^2 \tag{3.94}$$

The determination of the Sommerfeld enhancement is thus simply determined by the asymptotic behaviour of the solution Φ to equation (3.92).

Furthermore, the initial conditions for this equation cannot be arbitrary if the solution is to be regular. For our purposes the following initial conditions are useful;

$$\Phi_l(0) = 1 \qquad \Phi_l'(0) = -\frac{\mu\alpha}{p(l+1)}, \tag{3.95}$$

since then the behaviour of the differential equation at $x = 0$ is handled. The choice $\Phi_l(0) = 1$ is of course somewhat arbitrary but the second condition must always adjust to the value of the first condition to handle the behaviour at $x = 0$. The choice $\Phi_l(0) = 1$ has however no impact on the final result. This can be understood if one considers the fact that only the asymptotic behaviour of the solution is of importance as seen in (3.93) and (3.94).

4

Methods

As described in the previous chapter, the dark matter mass distribution, ρ_{DM}, the Sommerfeld enhancement factor, $S(v)$, and the dark matter velocity distribution $F(\mathbf{v})$ are needed to calculate the desired J_s-factor. The expression for the J_s-factor is repeated here for clarity:

$$J_s = \int_{\Delta\Omega} \int_{\text{l.o.s.}} \rho^2_{\text{DM}} \int F(\mathbf{v})\, S(\text{v})\, \text{d}^3\mathbf{v}\, \text{d}s\, \text{d}\Omega\,. \tag{4.1}$$

When these three components have been calculated, the three integrals can be performed to yield the J_s-factor. ρ_{DM} will be estimated using a maximum likelihood estimation outgoing from the l.o.s. velocity data for the stars in 20 dSphs (with the same data as in [9]). This estimation will be described in section 4.3. The calculation of the Sommerfeld enhancement factor and the dark matter velocity distribution is done numerically. In all calculations, *Mathematica* has been chosen as the numerical tool, while any scientific computation language should suffice. Our code is submitted in Appendix A. In section 4.6 a validation of our method is described as well as an approximate calculation of J_s-factors accounting for self-interaction used in previous research.

4.1 Numerical calculation of the Sommerfeld enhancement

The differential equation in (3.92) was solved numerically with $l = 0$, $p = 2\mu v$ and $\hbar = 1$:

$$\Phi_0'' + \frac{2}{x}\Phi_0' + (\frac{\alpha e^{-\frac{m_\phi}{2v}x}}{vx} + 1)\Phi_0 = 0, \tag{4.2}$$

and the boundary conditions

$$\Phi_0(0) = 1 \qquad \Phi_0'(0) = -\frac{\alpha}{mv}. \tag{4.3}$$

The value of α was set to $1/100$ and the mediator particle mass m_ϕ to $1\,\text{GeV/c}^2$ as in [8, 17]. Eq. (4.2) was solved parametrically in the relative velocity v and particle mass m.

The Sommerfeld enhancement was then acquired by:

$$S(v) = \left(\frac{1}{C}\right)^2, \tag{4.4}$$

where the C is given by the asymptotic sinusoidal behaviour of the solution to (4.2)-(4.3):

$$x\Phi_0(x) \to C\sin(x + \delta_0) \quad \text{as } x \to \infty. \tag{4.5}$$

Expressed in $\Phi_0(x)$, the Sommerfeld enhancement is calculated by:

$$S(v) = \lim_{x\to\infty} \frac{1}{\Big(x\Phi_0(x)\Big)^2 + \Big((x-\pi/2)\Phi_0(x-\pi/2)\Big)^2}, \tag{4.6}$$

Numerically, the expression in (4.6) was evaluated until the value did not change within the desired margin of error. A value of $x = 50$ was enough for our purposes, which yielded an accuracy of six digits.

4.2 Numerical calculation of the dark matter velocity distribution

Computing the dark matter velocity distribution includes many extensive computational steps, and therefore a simplifying numerical approach was used.

The main methodology used was to write all expressions dimensionless when possible, to simplify calculations. Furthermore, the amount of dependent parameters was reduced by applying certain scalings. We used r_0 and ρ_0 as length and density scales, respectively. This takes immediate effect in Ψ and ρ as

$$\begin{aligned} x &= \frac{r}{r_0} \\ \Psi(r) &= G\rho_0 r_0^2 \times \tilde{\Psi}(x) \\ \rho_{\mathrm{DM}}(r) &= \rho_0 \times \tilde{\rho_{\mathrm{DM}}}(x) \end{aligned} \tag{4.7}$$

where $\sim$ indicates a dimensionless function. This change of length variable will cause every derivative in r to yield a factor of r_0^{-1}, as per the chain rule. Numerically, this shows up when computing the distribution function $f(\mathcal{E})$ from equation (3.58). Thus, we arrived at the following quantities:

$$\begin{aligned} \mathcal{E}' &= \frac{1}{G\rho_0 r_0^2} \times \mathcal{E} \\ f(\mathcal{E}) &= \frac{r_0}{r_0^3 G\sqrt{G\rho_0 r_0^2}} \times \tilde{f}(\mathcal{E}') = r_0^{-3} G^{-\frac{3}{2}} \rho_0^{-\frac{1}{2}} \times \tilde{f}(\mathcal{E}') \end{aligned} \tag{4.8}$$

Here it should be noted that $\mathcal{E}'$ is not strictly dimensionless, as a consequence of the definition of $\mathcal{E}$ in equation (3.47), but instead has dimension M^{-1}. This is accounted

for in $\tilde{f}(\tilde{\mathcal{E}})$ however. Following the already presented theory, we then extracted the velocity distribution from this result. Given the energy scale set in equation (4.8) we constructed the velocity scale as

$$\tilde{v} = \frac{1}{\sqrt{G\rho_0 r_0^2}} \times v. \tag{4.9}$$

From this, we arrived at our final expression, now reduced to just depend on relative velocity, v_{rel} and the parameter x as follows:

$$F_x(v_{\text{rel}}) = \frac{1}{\sqrt{G\rho_0 r_0^2}} \times \tilde{F}_x(\tilde{v}_{\text{rel}}). \tag{4.10}$$

4.3 Likelihood estimation of the dark matter mass distribution

For this estimation, we assumed a Gaussian distribution for the l.o.s. stellar velocity data in the different dSphs. The resulting likelihood function, L, takes the form:

$$\mathcal{L} = -\log L = \frac{1}{2}\sum_{i=1}^{N_\star}\left[\frac{(v_i - u)^2}{\sigma_i^2} + \log\left(2\pi\sigma_i^2\right)\right] \tag{4.11}$$

The index i goes over the $N_\star$ stars in the sample, v_i is the particular l.o.s. velocity of one star and u is the mean of the l.o.s velocities in the data sample. The expected velocity dispersion squared, σ_i^2, is taken as the squared sum of the theoretical model of the velocity dispersion, $\sigma_{\text{los}}(R_i)$, and the measurement uncertainty, ϵ_i, in the velocity of a particular star: $\sigma_i^2 = \sigma_{los}^2(R_i) + \epsilon_i^2$. Here, R_i, is the projected radial distance of the star from the galactic centre.

We assumed the spherical Jeans equations described in section 3.3, which is standard in the field [9]. Also, we assumed an isotropic velocity dispersion, which corresponds to an anisotropy factor, β, equal to zero. Then, the theoretical velocity dispersion $\sigma_{los}(R_i)$ could be determined from the dark matter mass distribution. This connection is established by combining the equation for the l.o.s velocity dispersion derived in the previous chapter (eq. (3.11)) with the expression for $\nu_\star\langle v_r^2\rangle$ in eq. (3.36) to arrive at

$$\sigma^2_{\text{l.o.s.}}(R) = \frac{2}{I(R)}\int_R^\infty \frac{r}{\sqrt{r^2 - R^2}} dr \int_r^\infty \frac{\nu_\star(s) GM(s)}{s^2}\,\mathrm{d}s \tag{4.12}$$

For $\nu_\star$, the Plummer profile was used, where $(\alpha, \beta, \gamma) = (2, 5, 0)$ [23]. For ρ_{DM}, the NFW profile was used, where $(\alpha', \beta', \gamma') = (1, 3, 1)$ [24, 25]. These values are standard in the field and were chosen to be able to compare the results with another study when validating our method [9].

From the above, the likelihood depends on the parameters in $\nu_\star$ and ρ_{DM}. These are $r_\star$ and r_0, ρ_0 respectively. The likelihood does not depend on $\rho_\star$ since the $\rho_\star$ in $I(R)$ and $\nu_\star$ cancel out in $\sigma_{los}(R)$. Since the dark matter mass distribution was of primary interest, the parameter $r_\star$ was treated as a nuisance parameter. For each pair of r_0 and ρ_0, the nuisance parameter was chosen to maximise the likelihood function.

The likelihood L in eq. (4.11) was then maximised with respect to the parameters r_0 and ρ_0. The resulting two parameters were used with eq. (2.5) to yield the most likely dark matter mass distribution with respect to the data sample.

4.3.1 Reduction of parameters and singularity handling

The numerical computation of the l.o.s. velcoity dispersion was approached in the same fashion as in section 4.2. Thus to begin with, any quantity containing the three parameters r_0, $r_\star$ and R was simplified with a dependence on just two ratios: $R_x = R/r_0$ and $x_\star = r_\star/r_0$. This was extremely helpful in numerical calculations, as it was then sufficient to create tables of data values in 2 instead of 3 parameters.

Numerically computing the velocity dispersion, $\sigma^2_{\mathrm{l.o.s.}}$, as given by equation (4.12), also includes a singularity when $r = R$, which complicates the numerics. This were solved with a fairly simple change of variables. First, the ratio were expressed in the dimensionless quantities as

$$\frac{r}{\sqrt{r^2 - R^2}} = \frac{r_0}{\sqrt{r_0^2}} \frac{r}{\sqrt{r^2 - R^2}} = \frac{x}{\sqrt{x^2 - R_x^2}} \tag{4.13}$$

and then make the change of variables $u^2 = x^2 - R_x^2$ so that

$$\begin{aligned} x &= \sqrt{u^2 + R_x^2} \\ dx &= \frac{u}{\sqrt{u^2 + R_x^2}} du \\ \implies \frac{x}{\sqrt{x^2 - R_x^2}} dx &= du \end{aligned} \tag{4.14}$$

4.4 Perfoming the integrals to calculate the J_s-factor

The integrand in the J_s-factor depends on the radial distance from the galactic centre and the relative velocity. The relative velocity is already an integration variable so this was left as it was. The radial distance r however was parametrised in the line of sight and solid angle integration variables by using the law of cosines illustrated in figure 4.1:

$$r(s, \cos\alpha) = \sqrt{s^2 + D^2 - 2s\cos\alpha}. \tag{4.15}$$

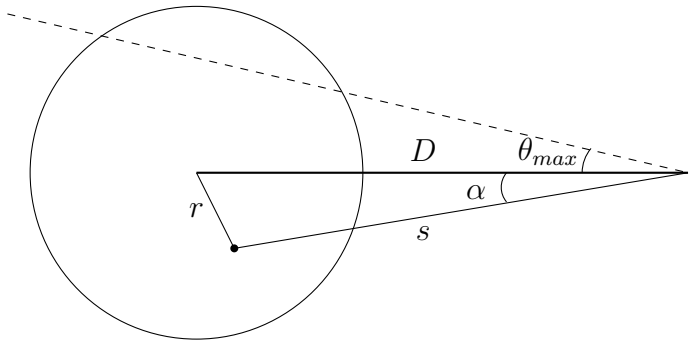

Figure 4.1: The galaxy seen from a distance D to it's centre, with the radial distance r from the galactic centre and the l.o.s. distance to the concerned star s in the galaxy. α is the angle between D and s and θ_{max} is the upper limit for the angular integration.

The integration in the line of sight variable s was then taken from 0 to ∞. In the solid angle integral, the variable $\gamma = \cos\alpha$ was integrated from $\cos\theta_{\max}$ to 1 and a factor of 2π was extracted from the azimuthal angular part. The upper integration limit for the angle, θ_{max}, was taken to be $0.5\,^\circ$. This angle covers approximately half of the luminosity in most of the dSphs [9]. It is appropriate to calculate the J-factor within this region, since the Jeans equations are most valid there [26, 27]. The integral parametrisation yielded the final numerical expression for J_s:

$$J_s = 2\pi \int_{\cos\theta_{\max}}^{1} \int_0^\infty \rho_{\mathrm{DM}}^2(r(s,\gamma)) \int_0^{10v_0} F_{r(s,\gamma)}(v_{\mathrm{rel}})\, S(v_{\mathrm{rel}})\, \mathrm{d}v_{\mathrm{rel}}\, \mathrm{d}s\, \mathrm{d}\gamma \tag{4.16}$$

where the upper integration limit in $\mathrm{d}v_{\mathrm{rel}}$ has been taken as

$$10v_0 = 10\sqrt{G\rho_0 r_0^2} \lessapprox \sqrt{8\tilde{\Psi}(x)}\sqrt{G\rho_0 r_0^2} \tag{4.17}$$

which should suffice, considering the constraints on v_{rel} discussed in section 3.4.3.

4.5 Calculation of confidence intervals for the J_s-factor

A grid in the two variables ρ_0 and r_0 was created and the likelihood function was calculated in every point. Each pair of ρ_0 and r_0 corresponds to one J_s in eq. (4.16). The likelihood and J_s for these pairs was plotted in a diagram. Data binning was used to select certain values of J_s: The range of J_s was divided in small intervals and in each interval the J_s with the maximum likelihood was chosen. This binning process allowed for a one-to-one relationship between the likelihood function L and the chosen J_s. From this, a test statistics was formed according to:

$$TS(J_s) = -2\log\frac{L(J_s)}{L_{max}}, \tag{4.18}$$

where L_{max} is the value of the absolute maximum likelihood for any pair ρ_0 and r_0. The confidence levels were then calculated using the chi-squared distribution with one degree of freedom.

4.6 Validation of method and complementary calculations

The validation of our likelihood estimation of J_s was made by calculating an likelihood estimation of the J-factor without self-interaction using the same likelihood estimation technique and comparing this to Chiappo et. al [9]. The J-factor without self-interaction was computed by setting the Sommerfeld enhancement to unity, making the velocity integral equal to 1 in 4.16.

To validate that the calculations of the Sommerfeld enhancement factor $S(v)$ and the dark matter velocity distribution $F(\mathbf{v})$ are correct, the results was compared to other studies [16, 17]. Also, as a sanity check, the integral of $F(\mathbf{v})$ was evaluated for each radial distance from the galactic centre to compare how close this value is to 1.

For further analysis, J_s was calculated for constant Sommerfeld enhancement, $S(v^*)$. This is a standard calculation for J-factors accounting self-interaction, for example in [28]. The enhancement becomes constant when considering only the mean velocity of the stars in the galaxy, i.e. no consideration of the distribution of velocities. Typical values for $v*$ in dSphs are 10^{-5} in units of c [21].

5

Results

We start by presenting the comparisons with previously published articles. The computation of $\mathcal{J}_s$-factors includes contribution of a Sommerfeld enhancement weighted with a velocity distribution. The validity of these two functions will be evaluated in the second section. In the third section we present the J_s-factor for the dSphs around the Milky Way.

5.1 Validation of statistical method

A likelihood-based method to determine J-factors without self-interaction has been used in Chiappo et al. [9]. Their method differs only by our use of $r_\star$ (the scale radius of the luminosity profile) alone as nuisance parameter instead of both $r_\star$ and r_0 (the scale radius of the dark matter profile). To evaluate our statistical method we compare our $\mathcal{J}$-factors with $S(v) = 1$ to their result. $\log_{10}(J)$ is denoted with $\mathcal{J}$ and the likelihood with L, and thereby $\log(L)$ with $\mathcal{L}$.

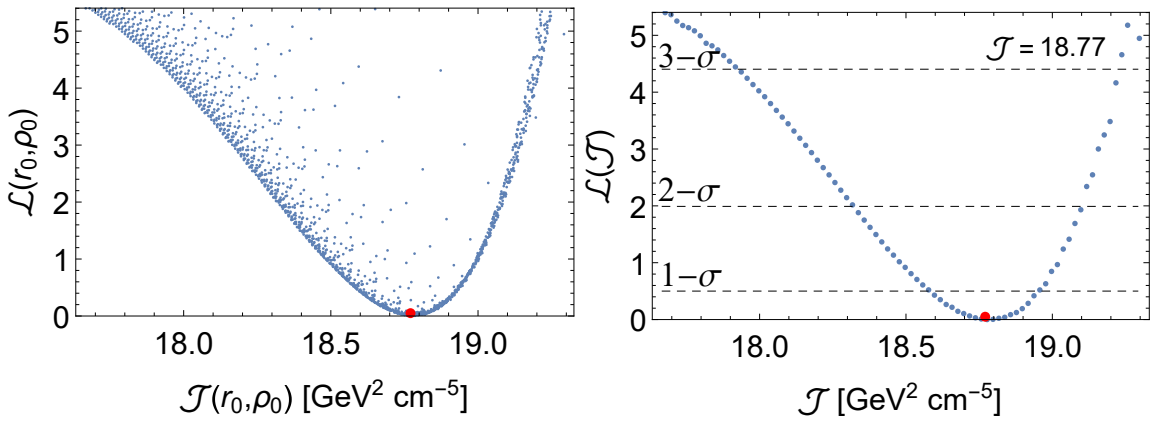

Figure 5.1: The left figure shows all likelihood values less than 5 relative to the minimum value. The variable r_0 range from 0.05 to 20 kpc and ρ_0 from 10^5 to 10^9 $M_\odot$kpc^{-3}. In the right figure a data binning method has been applied to select the points with the lowest likelihood. The minimum likelihood is found $\mathcal{J}$ of 18.77.

Table 5.1 shows the discrepancy with Chiappo et al. for 20 dSph. The seven galaxies above the dashed line has a $\mathcal{J}$ that lies within the 1-σ from the $\mathcal{J}$ in Chiappo et al. Our $\mathcal{J}$ for Draco differs with 4% and Segue 1 differs with 18% [9]. For four of the galaxies below the dashed line, the 1-σ intervals overlap. These are Coma Berenices, Canes Venatici II, Bootes II and Ursa Major II. For some of the galaxies one of the 1-σ interval limits are not existing due to lack of data points.

Table 5.1: Table comparing J-factors with Chiappo et al. [9]. Galaxies above the dashed line have a $\mathcal{J}$ which include the $\mathcal{J}$ from [9] within 1-σ. Missing 1-σ-levels are indicated with "-". The difference is given as $\Delta\mathcal{J}$, the $\log_{10}$ of the ratio between our and the referred J-factors. The last three columns are the optimised values for $r_\star$, r_0 and ρ_0.

Galaxy	$\mathcal{J}$ [GeV^2 cm^{-5}]	$\Delta\mathcal{J}$	r_* [kpc]	r_0 [kpc]	ρ_0 [$M_\odot$kpc^{-3}]
Draco	$18.77^{+0.16}_{-0.19}$	-0.02	0.21	14.95	$1.79 \cdot 10^6$
Leo I	$17.70^{+0.18}_{-0.18}$	-0.03	0.37	9.90	$1.79 \cdot 10^6$
Ursa Major I	$17.94^{+0.64}_{-0.91}$	-0.09	0.48	0.21	$2.26 \cdot 10^8$
Leo IV	$16.54^{+0.82}_{-1.33}$	-0.19	0.24	0.21	$7.39 \cdot 10^7$
Willman 1	$19.60^{+0.37}_{-0.33}$	-0.26	0.029	17.98	$2.60 \cdot 10^6$
Leo T	$16.38^{+1.21}_{-0.72}$	-0.55	1.86	0.21	$1.71 \cdot 10^8$
Segue 1	$18.67^{+0.82}_{-2.37}$	-0.75	0.085	0.21	$1.29 \cdot 10^8$
Sculptor	$18.87^{+0.14}_{-}$	0.17	0.11	0.61	$1.18 \cdot 10^8$
Coma Berenices	$19.42^{+0.22}_{-0.21}$	0.37	0.0033	1.82	$2.92 \cdot 10^7$
Carina	$17.52^{+0.23}_{-0.27}$	-0.39	0.52	20	$3.35 \cdot 10^5$
Canes Venatici II	$18.37^{+0.32}_{-0.27}$	0.54	0.016	13.13	$1.96 \cdot 10^6$
Sagittarius	$20.34^{-}_{-0.13}$	0.57	0.079	1.01	$1.18 \cdot 10^8$
Bootes II	$19.22^{+0.40}_{-3.33}$	0.58	0.026	17.78	$1.79 \cdot 10^6$
Ursa Major II	$19.89^{+0.24}_{-0.30}$	0.63	0.0033	2.83	$2.42 \cdot 10^7$
Canes Venatici I	$18.08^{-}_{-0.23}$	0.75	0.037	0.21	$6.28 \cdot 10^8$
Ursa Minor	$19.48^{-}_{-0.37}$	0.84	0.024	0.21	$9.11 \cdot 10^8$
Fornax	$17.09^{+0.10}_{-0.04}$	-0.95	1.97	9.50	$6.43 \cdot 10^5$
Sextans	$18.77^{+0.08}_{-}$	1.01	0.05	0.21	$5.21 \cdot 10^8$
Bootes I	$17.93^{+0.40}_{-0.45}$	1.11	0.0044	2.83	$4.13 \cdot 10^6$
Hercules	$18.50^{+0.16}_{-0.17}$	1.17	0.036	20	$1.35 \cdot 10^6$

A further investigation of the likelihood on the parameter space $\{r_0, \rho_0\}$, as in figure 5.2, shows a long flat valley for the likelihood. However, the $\mathcal{J}$-factors in fig. 5.1 have a similar structure. $\mathcal{J}$ gets a well defined maximum likelihood value as seen in the right of fig. 5.1.

Some error estimations for the galaxies in table 5.1 gives unevaluated 1-σ levels. One such galaxy is Canes Venatici I, seen in fig. 5.3. The left plot is a contour plot over r_0 and ρ_0, showing the 1,2,3-σ error estimations and $\mathcal{J}$-values. The right plot is the likelihood and $\mathcal{J}$, both calculated in the $\{r_0, \rho_0\}$-space.

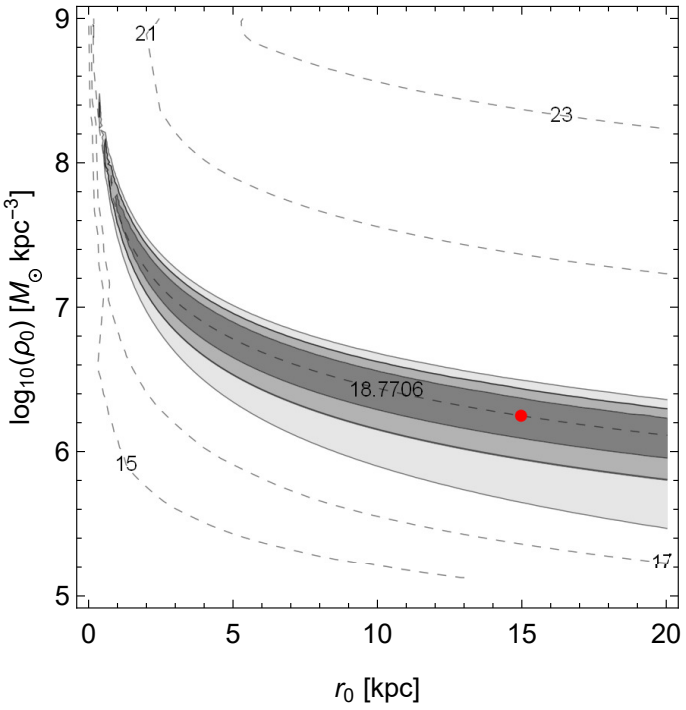

Figure 5.2: Dashed contours specifying $\mathcal{J}$ values in the r_0 and ρ_0 plane. The grey boundaries defines confidence intervals from darker to lighter: 1-σ, 2-σ and 3-σ. The confidence intervals are constructed from calculation on Draco but the principle of a long flat valley is characteristic.

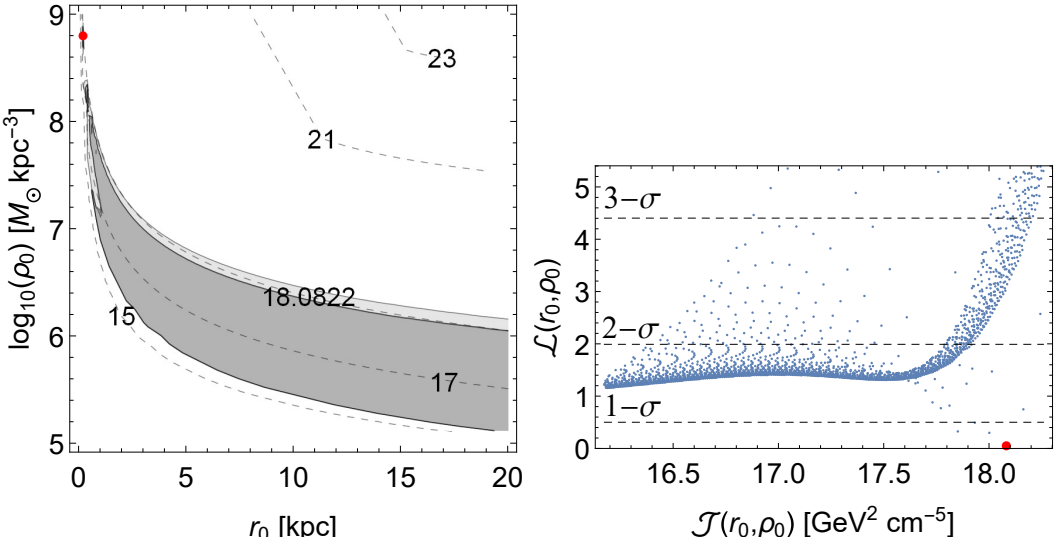

Figure 5.3: The left plot shows the likelihood error estimation 1,2,3-σ from darker to lighter shades of grey with the minimum showed by a red dot. $\mathcal{J}_s$ values are showed with dashed lines. The right hand plot shows the likelihood versus the $\mathcal{J}$ value and gives the error estimations in levels of 1,2,3-σ. Both plots are for data from Canes Venatici I, giving an example for a galaxy with an inconsistent error estimation.

5.2 Validation of the Sommerfeld enhancement and the velocity distribution

The Sommerfeld enhancement is dependent of two parameters, the particle mass and velocity, and thus two figures are presented for evaluation of its validness. First fig. 5.4 shows the dependence of the particle's mass. This can be compared with the results in Robertson and Zentner [17]. A comparison shows a similar behaviour in the particle mass parameter, for example both have a resonance peak at 650 GeV/c^2 with an enhancement of $2 \cdot 10^5$.

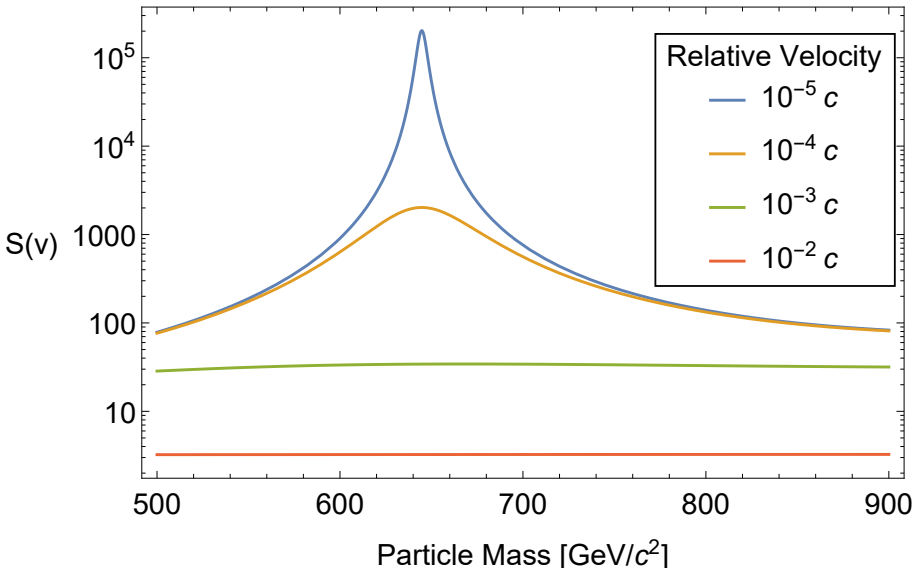

Figure 5.4: Sommerfeld enhancement factor for four different velocities as a function of particle mass. Here $\alpha = \frac{1}{100}$ and $m_\phi = 1\,\mathrm{GeV/c^2}$. The resonance peak around 650 GeV/c^2 is very dominant for low velocities, but vanishes for velocities over 10^{-3} c.

The Sommerfeld enhancement's velocity dependence for different masses is described in the fig. 5.5. Velocities above 0.001 c gives the same enhancement and for small velocities the enhancement becomes constant. For the yellow line, which represents a mass of 650 GeV/c^2, the enhancement is almost 10^5. This is consistent with Robertson and Zentner [17].

The velocity distribution shall by construction integrate to 1 for a given radius, and fig. 5.6 states that our distribution satisfies this to four digits. The distribution is higher and more narrow for smaller velocities and agrees with Ferrer and Hunter [16].

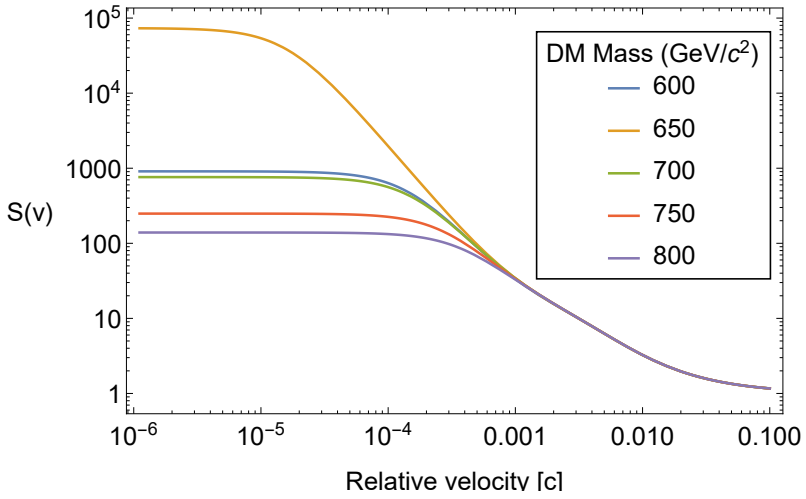

Figure 5.5: Sommerfeld enhancement factor for five different masses as a function of relative velocity. Here $\alpha = \frac{1}{100}$ and $m_\phi = 1\,\mathrm{GeV/c^2}$. For all masses, the enhancements approach a constant value for low velocites.

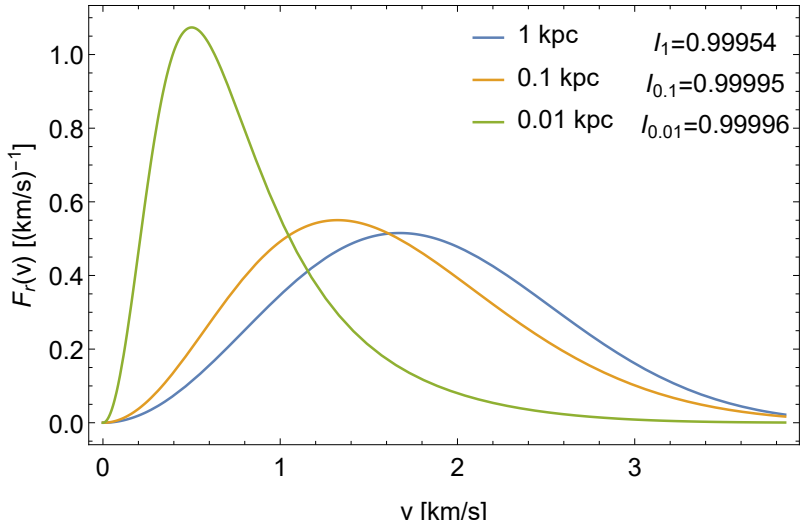

Figure 5.6: Velocity distribution calculated from Eddington inversion formula, using typical values of $r_0 = 0.6$ and $\rho_0 = 3.6 \cdot 10^5$, with emphasis on that the feature but not scale is preserved when considering different parameters. For smaller radii the distribution becomes more narrow and higher, giving more weight to lower velocities. The integral for each curve is specified in the graph and is equal to unity.

5.3 J_s-factors for dSphs including self-interaction

The computation of $\mathcal{J}_\mathrm{s}$ is compared with $\mathcal{J}_\mathrm{s}^{S(v^*)}$ (where the Sommerfeld enhancement is constant) in table 5.2. For Draco $J_\mathrm{s}^{S(v^*)}$ is about 17 times larger than J_s. The table also states J-factors without Sommerfeld enhancement for comparison.

Table 5.2: Calculated $\mathcal{J}$, $\mathcal{J}_\mathrm{s}$ and $\mathcal{J}_\mathrm{s}^{S(v^*)}$, and in the last column $\Delta\mathcal{J}$ for $\mathcal{J}_\mathrm{s}$ and $\mathcal{J}_\mathrm{s}^{S(v^*)}$. The galaxies have the same order as in table 5.1 and "-" are indicating missing 1-σ-levels.

Galaxy	$\mathcal{J}$	$\mathcal{J}_\mathrm{s}$	$\mathcal{J}_\mathrm{s}^{S(v^*)}$	$\mathcal{J}_\mathrm{s} - \mathcal{J}_\mathrm{s}^{\mathrm{S(v*)}}$
Draco	18.77	$22.26^{+0.29}_{-0.13}$	23.50	-1.24
Leo I	17.70	$21.13^{+0.31}_{-0.16}$	22.43	-1.30
Ursa Major I	17.94	$22.13^{+0.44}_{-0.91}$	22.67	-0.54
Leo IV	16.54	$21.00^{+0.59}_{-1.39}$	21.27	-0.27
Willman 1	19.60	$23.08^{+0.32}_{-0.21}$	24.33	-1.25
Leo T	16.38	$20.69^{+0.82}_{-1.04}$	21.11	-0.42
Segue 1	18.67	$23.00^{+0.57}_{-2.12}$	23.40	-0.40
Sculptor	18.87	$22.62^{+0.15}_{-}$	23.60	-0.98
Coma Berenices	19.42	$23.05^{+0.10}_{-0.17}$	24.15	-1.10
Carina	17.52	$21.38^{+0.23}_{-0.18}$	22.26	-0.87
Canes Venatici II	18.37	$21.72^{+0.24}_{-0.19}$	23.10	-1.37
Sagittarius	20.34	$23.89^{-}_{-0.10}$	25.07	-1.18
Bootes II	19.22	$22.80^{+0.38}_{-2.36}$	23.95	-1.15
Ursa Major II	19.89	$23.43^{+0.22}_{-0.17}$	24.62	-1.19
Canes Venatici I	18.08	$22.00^{-}_{-0.26}$	22.81	-0.81
Ursa Minor	19.48	$23.27^{-}_{-0.74}$	24.21	-0.94
Fornax	17.09	$20.94^{+0.09}_{-0.08}$	21.82	-0.88
Sextans	18.77	$22.73^{+0.05}_{-}$	23.50	-0.77
Bootes I	17.93	$21.89^{+0.24}_{-0.39}$	22.66	-0.77
Hercules	18.50	$21.82^{+0.10}_{-0.11}$	23.23	-1.41

Fig. 5.7 for J_s shows a great similarity with fig. 5.2 and 5.1 (for the J-factor without Sommerfeld enhancement). The difference is larger $\mathcal{J}$ values. All mentioned figures has data from Draco.

In table 5.2 there is an overestimation for all galaxies when using a constant velocity for the Sommerfeld enhancement, $\mathcal{J}_\mathrm{s}^{S(v^*)}$, compared with the calculation encountering for the velocity distribution, $\mathcal{J}_\mathrm{s}$. For Draco we made a more extensive investigation by using dark matter particle masses between 500 and 800 $\mathrm{GeV/c^2}$, as suggested in our chosen model [8]. By using the best fitted parameters $r_0 = 14.95\,\mathrm{kpc}$ and $\rho_0 = 1.79 \cdot 10^6\,\mathrm{M} \odot\,\mathrm{kpc}^{-3}$, the difference is shown in fig. 5.8. Depending on different masses we get an enhancement up to 1.5 orders of magnitudes larger for $\mathcal{J}_\mathrm{s}^{S(v^*)}$.

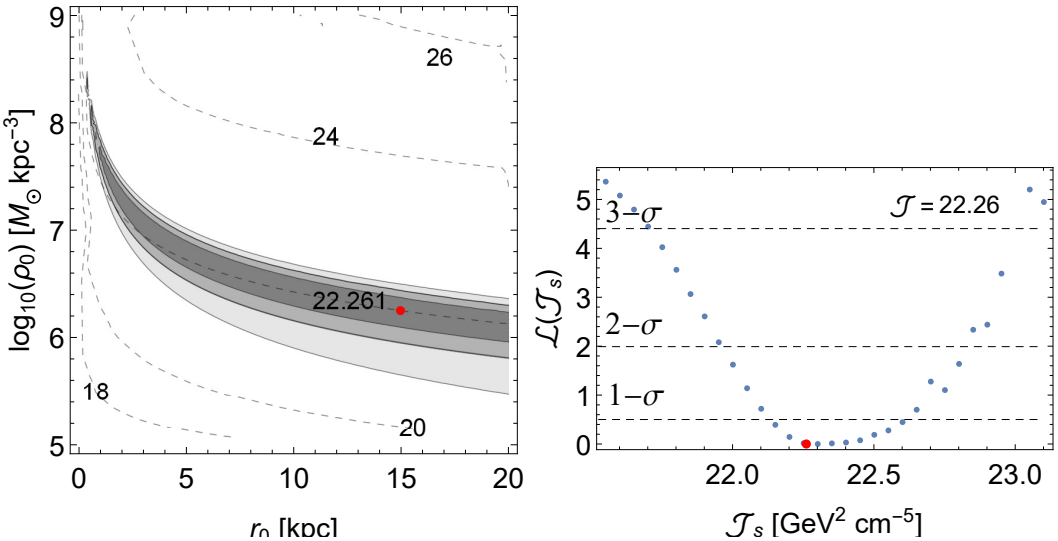

Figure 5.7: The left plot shows the likelihood error estimation $1, 2, 3 - \sigma$ from darker to lighter shades of grey with the minimum showed by a red dot. $\mathcal{J}_s$ values are showed with dashed lines. The right hand plot shows the likelihood versus the $\mathcal{J}_s$ value and indicates the error estimations in levels of $1, 2, 3 - \sigma$. Both plots are for data from Draco.

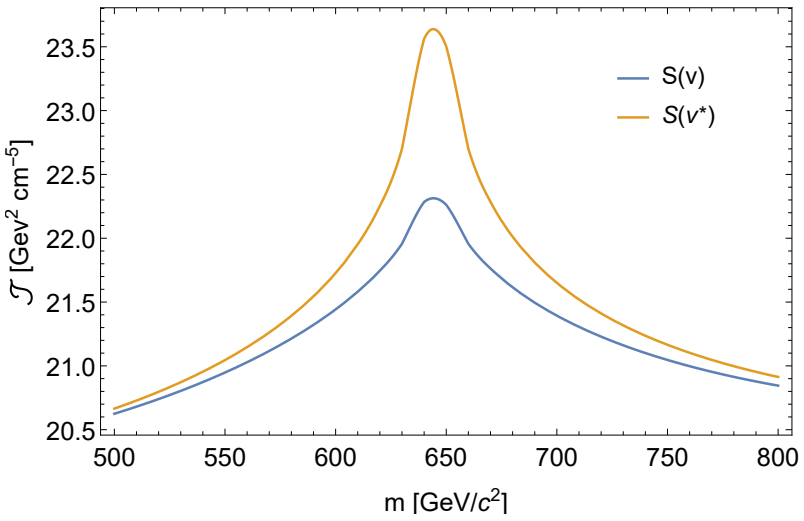

Figure 5.8: A comparison of $\mathcal{J}$ values when using a constant velocity or the velocity distribution for the Sommerfeld enhancement for Draco. Constant Sommerfeld enhancement, using ($v^* = 10^{-5}c$), is shown with the orange line, and accounting for the velocity distribution, is shown with the blue line.

6

Discussion

We divide the discussion into two parts, one for the validation of our method and one where we discuss the differences between the J-factors.

6.1 Comparison with previous results

In the results we compare $\mathcal{J}$ with previously published results from Chiappo et al. in table 5.1. We notice that 16 of Chiappo's J-factors lies within our 2-σ-levels for the respective J_s with $S(v) = 1$. For 11 of these, our 1-σ-intervals overlap with theirs. This verifies that the maximum likelihood estimation used in our calculation of the J_s-factors is reasonable.

As mentioned before, we use one nuisance parameter, $r_\star$, while Chiappo et al. uses two, $r_\star$ and r_0. With our method, the maximisation of the likelihood is more constrained since Chiappo eliminates two parameters before this process and we only eliminate one. Due to this, the likelihood valley is much shallower than Chiappo's. This is also seen in the comparison as our confidence intervals are generally larger.

As for the likelihood estimation, a Gaussian distribution for the l.o.s. stellar velocity data was assumed. The true stellar velocity dispersion in some dSphs, for example ultra-faint dwarfs, is similar to the measurement uncertainty [9]. Thus the expected velocity dispersion highly depends on Gaussian measurement uncertainty and the assumption must at least be a good approximation. In future research other velocity distributions other than Gaussian might be of interest.

The 1-σ-levels marked with "-" in table 5.1 are not well-defined for the grid in parameter space used in our analysis. As such, these 1-σ-levels could not be retrieved by the used method. One could however calculate these using a different grid in parameter space from $\{r_0, \rho_0\}$, more centred around the region of importance. This would allow for extraction of more relevant data points so that the binning process produces a continuous likelihood curve of $\mathcal{J}$.

In table 5.1 there is a wide range in the galactic parameters, $r_\star$, r_0 and ρ_0. As shown in fig. 5.2 the J-factors are not affected much when following likelihood contours, i.e. changing the parameters while maintaining constant J. The same is true for the J_s-factors as shown in fig. 5.7. Furthermore, there is a lack of published research that determines the constraints on galactic parameters for dSphs, both in specific galaxies

and generally. Such research could be of interest, especially for those galaxies with unidentified 1-σ levels. These constraints can be used to focus the analysis on a certain parameter range and increase the amount of likelihood estimations around the maximum likelihood in the data in fig. 5.3. The data binning will then be more compatible with a 1-σ level determination.

6.2 The impact of a proper velocity distribution

We have studied the generalised J-factor in different situations. The classical approach without self-interaction has been extensively covered in the last section with comparisons to previous research. Here, we compare the rigorous J_s-factor to the previously used approximation of a constant Sommerfeld enhancement factor to evaluate the differences from when one uses a proper velocity distribution [28].

As shown in table 5.2 there is a significant increase of 3 to 4 orders of magnitude (depending on which galaxy) in the J-factor when introducing self-interaction. An increase in the factor is of course expected as the Sommerfeld enhancement factor for an attractive potential is always 1 or larger, but this fact does not fully explain the difference of 3 to 4 orders of magnitude. It can however be explained by the chosen dark matter particle mass used in the analysis. We have assumed a particle mass of $650\,\mathrm{GeV/c^2}$ which, as can be seen in fig. 5.4, corresponds to a resonance peak with significantly higher Sommerfeld enhancement values. This resonance peak could be a factor of great importance in future indirect dark matter searches, as a very high observed gamma ray flux could indicate dark matter masses in the region of a resonance peak. On the other hand, outside the resonance peaks the Sommerfeld enhancements for different masses quickly reaches fairly similar values, and as such, determining a hypothetical dark matter mass in those regions might be significantly harder.

Whether one should include the velocity distribution or not when calculating $\mathcal{J}_s$ is due to two aspects, namely which particle mass and which galactic parameters (r_0 and ρ_0) that is of interest. Particle masses in a resonance peak gives a large overestimation of $\mathcal{J}_s^{S(v^*)}$ as shown in fig. 5.8. However, one can see in the same figure that if particle masses far away from resonance peaks are of interest the two calculations are almost equal. Furthermore, in fig. 5.5 one can see that the Sommerfeld enhancement becomes constant for low speeds, from 10^{-4} c to 10^{-5} c dependent on particle mass. So if no higher speeds are of consideration there will be no need to perform the $\mathcal{J}_s$ with the velocity distribution. This is the case for small galaxy radii, where the velocity is lower, as seen in fig. 5.6.

7

Conclusion

In this thesis we present an ab initio approach to calculate a more general J-factor for dwarf spheroidal galaxies. This generalisation takes self-interaction between dark matter particles into account in a more rigorous manner than before.

We can conclude that if dark matter particles has the properties of self-interaction, the J-factors significantly increases from $10^{17}-10^{20}$ to $10^{21}-10^{24}$ for dwarf spheroidal galaxies. Furthermore, we conclude that the standard approximative calculation, using a constant Sommerfeld enhancement, overestimated the J_s-factor of up to 1.5 orders of magnitude.

We verify that the maximum likelihood estimation used in our calculation of the J_s-factors is reasonable. By comparison with calculations of J-factors without self-interaction, the confidence intervals are larger. This is due to the inevitable constraints appearing in the parameter space when considering self-interaction.

During the completion of this thesis another report with a similar purpose was uploaded on arXiv.org, [29]. An important difference between our studies lies in the solution of the Schrödinger equation including a Yukawa potential. They use an approximation allowing an analytical solution of the Schrödinger equation. We use a numerical approach to solve the full Schrödinger equation. Our method introduces numerical difficulties but gives more accurate results.

References

[1] M. Ackermann et al., "Dark matter constraints from observations of 25 milky way satellite galaxies with the fermi large area telescope", Physical Review D **89** (2014).

[2] G. Bertone and D. Hooper, "A history of dark matter", (2016).

[3] D. D. R. Williams, *Planetary fact sheet*, NASA Space Data Coordinated Archive, (Dec. 2016) `https://nssdc.gsfc.nasa.gov/planetary/factsheet/`.

[4] M. Milgrom, "The mond paradigm", (2008).

[5] D. Clowe, A. Gonzalez, and M. Markevitch, "Weak-Lensing Mass Reconstruction of the Interacting Cluster 1E 0657-558: Direct Evidence for the Existence of Dark Matter", Astrophysical Journal **604**, 596 (2004).

[6] M. H. Jones, R. J. Lambourne, S. Serjeant, and O. University, *An introduction to galaxies and cosmology*, 2nd edition (Cambridge University Press, Cambridge, 2015).

[7] M. Kamionkowski, "Wimp and axion dark matter", (1997).

[8] N. Arkani-Hamed, D. P. Finkbeiner, T. R. Slatyer, and N. Weiner, "A theory of dark matter", Phys. Rev. D **79**, 015014 (2009).

[9] A. Chiappo et al., "Dwarf spheroidal j-factors without priors: a likelihood-based analysis for indirect dark matter searches", Monthly Notices of the Royal Astronomical Society **466**, 669 (2016).

[10] L. Hui, "Unitarity bounds and the cuspy halo problem", Physical Review Letters **86**, 3467 (2001).

[11] A. Loeb and N. Weiner, "Cores in dwarf galaxies from dark matter with a yukawa potential", Physical Review Letters **106**, 171302 (2011).

[12] A. Geringer-Sameth et al., "Indication of gamma-ray emission from the newly discovered dwarf galaxy reticulum ii", PHYSICAL REVIEW LETTERS **115**, 081101 (2015).

[13] D. Harvey et al., "The non-gravitational interactions of dark matter in colliding galaxy clusters", (2015).

[14] R. G. Dubinski John; Carlberg, "The structure of cold dark matter halos", Astrophys.J (1991).

[15] D. N. Spergel and P. J. Steinhardt, "Observational evidence for self-interacting cold dark matter", Physical Review Letters (1999).

[16] F. Ferrer and D. R. Hunter, "The impact of the phase-space density on the indirect detection of dark matter", Journal of Cosmology and Astroparticle Physics **2013** (2013).

[17] A. R. Z. Brant E. Robertson, "Dark matter annihilation rates with velocity-dependent annihilation cross sections", Phys. Rev. D (2009).
[18] J. Binney and S. Tremaine, *Galactic dynamics* (Princeton University Press, Princeton, New Jersey, 1987).
[19] K. S. Krane, *Introductory nuclear physics, 2nd ed.* (John Wiley & Sons, Inc., 1988).
[20] J. J. Sakurai and J. Napolitano, *Modern quantum mechanics*, 2nd edition, Pearson new international (Pearson, Harlow, 2014).
[21] R. Iengo, "Sommerfeld enhancement: general results from field theory diagrams", Journal of High Energy Physics **2009**, 024 (2009).
[22] L. Landau and E. Lifshitz, *Quantum mechanics: non-relativistic theory* (Pergamon Press, 1965).
[23] H. C. Plummer, "On the problem of distribution in globular star clusters", Monthly Notices of the RAS **71**, 460 (1911).
[24] H. Zhao, "Analytical models for galactic nuclei", Monthly Notices of the Royal Astronomical Society **278**, 488 (1996).
[25] J. F. Navarro, C. S. Frenk, and S. D. M. White, "A universal density profile from hierarchical clustering", The Astrophysical Journal **490**, 493 (1997).
[26] J. Wolf et al., "Accurate masses for dispersion-supported galaxies", Monthly Notices of the Royal Astronomical Society **406**, 1220 (2010).
[27] M. G. Walker et al., "Dark matter in the classical dwarf spheroidal galaxies: a robust constraint on the astrophysical factor for gamma-ray flux calculations", The Astrophysical Journal Letters **733**, L46 (2011).
[28] M.-H. Chan, "Does the gamma-ray signal from the central milky way indicate sommerfeld enhancement of dark matter annihilation", (2016).
[29] K. K. Boddy, J. Kumar, L. E. Strigari, and M.-Y. Wang, "Sommerfeld-enhanced j-factors for dwarf spheroidal galaxies", (2017).

A

Mathematica code

Here we present the MATHEMATICA code used in the project.

A.1 Interpolated velocity dispersion function

σ^2_{los} Interpolated Function

```
ClearAll["Global`*"]
```

Constants

```
points = 700;

pi = 3.141593; (*giving π in floating form to speed up computation*)

(*Galactic parameters*)
αBrightness = 2.;
βBrightness = 5.;
γBrightness = 0.;
αDM = 1.;
βDM = 3.;
γDM = 1.;

(*Parameter space of interest*)
RMin = 10^-4;
RMax = 6;
r0Min = 5. * 10^-3;
r0Max = 20.;
rStarMin = 10^-3;
rStarMax = 2.;


timeOnePoint = 0.3 / 3600; (*hours*)
time = 12 (*hour*)
n = N[(time / timeOnePoint)^(1/2)]
```

Equations

All lengths in units of r0;

$x = \frac{r}{r0}$

$Rx = \frac{R}{r0}$

$$\frac{x}{\sqrt{x^2-Rx^2}} = \frac{r/r0}{\sqrt{r/r0^2-R/r0^2}} = \frac{r}{\sqrt{r^2-R^2}}$$

```
losProjection[x_, Rx_] := x / Sqrt[x^2. - Rx^2.];

generallDensityFunction[r_, r0_, ρ0_, α_, β_, γ_] := ρ0 (r/r0)^-γ (1. + (r/r0)^α)^-((β-γ)/α)
```

$\rho_{DM}(r) = \rho 0$ rhoDM$\left[\frac{r}{r0}\right]$

```
rhoDM[x_] = generallDensityFunction[x, 1., 1., αDM, βDM, γDM];
```

$v(r, \text{rStar}) = v0\ \text{nuStar}\left[\frac{r}{\text{r0}}, \frac{\text{rStar}}{\text{r0}}\right]$

$x = \frac{r}{\text{r0}}$

$\text{rStarDividedr0} = \frac{\text{rStar}}{\text{r0}}$

```
nuStar[x_, rStarDividedr0_] = generallDensityFunction[
   x, rStarDividedr0, 1., αBrightness, βBrightness, γBrightness];
```

$\text{I(R,rStar)} = v0 * \text{r0}\ \text{surfaceBrightness}\left[\frac{\text{R}}{\text{r0}}, \frac{\text{rStar}}{\text{r0}}\right]$

$\text{Rx} = \frac{R_x}{\text{r0}}$

$\text{rStarDividedr0} = \frac{\text{rStar}}{\text{r0}}$

```
surfaceBrightness[Rx_, rStarDividedr0_] = FullSimplify[
   2. * Integrate[nuStar[x, rStarDividedr0] * losProjection[x, Rx], {x, Rx, ∞}]
   , Rx > 0 && rStarDividedr0 > 0];
```

$\text{M(s)} = G\,\rho 0 * \text{r0}^3\ \text{massintegral}\left[\frac{s}{\text{r0}}\right],$

$\text{sx} = \frac{s}{\text{r0}}$

```
massIntegral[sx_] = FullSimplify[
   4. * pi * Integrate[rhoDM[x] * x^2, {x, 0., sx}]
   , sx > 0];
```

$\sigma^2_{\text{los}}\text{(R,rStar)} = \frac{1}{v0\,\text{r0}} * v0 * G\,\rho 0\ \text{r0}^3\ \frac{1}{\text{r0}^2}$ * r0*r0 2 **σLosSquared[**$\frac{R}{\text{r0}}, \frac{\text{rStar}}{\text{r0}}$**]=**

2 G ρ**0** r0^2**σLosSquared[**$\frac{R}{\text{r0}}, \frac{\text{rStar}}{\text{r0}}$**]**

$x = \frac{s}{\text{r0}}$

$\text{x2} = \frac{r}{\text{r0}}$

$\text{Rx} = \frac{R}{\text{r0}}$

$\text{rStarDividedr0} = \frac{\text{rStar}}{\text{r0}}$

$\text{x2}^2 = u^2 + \text{Rx}^2 \text{ -> dx2} = \frac{u}{\sqrt{\text{x2}^2 + \text{Rx}^2}}$

```
σLosSquared2Parameter[Rx_, rStarDividedr0_] :=
 1/surfaceBrightness[Rx, rStarDividedr0] * NIntegrate[
   1/x^2 nuStar[x, rStarDividedr0] * massIntegral[x],
   {u, 10^-5, ∞}, {x, Sqrt[u^2 + Rx^2], ∞}, Method →
    {"GlobalAdaptive", "SymbolicProcessing" → 0, "SingularityDepth" → 1000000000},
   MinRecursion → 20, MaxRecursion → 100, AccuracyGoal → 6, PrecisionGoal → ∞]
```

Table and Export

σ^2_{los}=2 ρ0 G r0^2 σLosSquared2ParameterIP[Rx,rStarDividedr0], **Notice that the exported function is only near to the correct** σ^2_{los}.

$\text{R} \in [2 * 10^{-4}, 5.5]$

$\text{rStar} \in [5 * 10^{-2}, 1]$

$r0 \in \left[5 * 10^{-2}, 10\right]$

```
points = 700;
RxMin = RMin / r0Max;

RxMax = RMax / r0Min;

rStarDividedr0Min = rStarMin / r0Max;

rStarDividedr0Max = rStarMax / r0Min;

stepSizeRx = (RxMax^(1/10) - RxMin^(1/10)) / (points - 1);
stepSizerStarDividedr0 = (rStarDividedr0Max^(1/10) - rStarDividedr0Min^(1/10)) / (points - 1);

σTableNFW =
  ParallelTable[
   {{Rx^10, rStarDividedr0^10}, σLosSquared2Parameter[Rx^10, rStarDividedr0^10]},
   {Rx, RxMin^(1/10), RxMax^(1/10), stepSizeRx},
   {rStarDividedr0, rStarDividedr0Min^(1/10),
    rStarDividedr0Max^(1/10), stepSizerStarDividedr0}];

SetDirectory[NotebookDirectory[]];
Flatten[σTableNFW, 1] >> "σTableNFW_700"
```

A.2 Maximum likelihood estimation for galactic parameters

```
ClearAll["Global`*"]

galaxyArray = {"booI", "booII", "com", "cvnI", "cvnII", "dra", "her", "leoIV", "leoT",
    "seg1", "umaI", "umaII", "umi", "wil1", "car", "for", "leoI", "scl", "sex", "sgr"};
 (*"car","for","leoI","scl","sex","sgr", samtliga av dessa kan
 komma att inte fungera och ligger därför sist*)

pi = 3.1415926536;

G = 4.2994 * 10^-6;
αDM = 1;
βDM = 3;
γDM = 1;
θMax = 0.5/180 pi;
 (* kpc, distance to galaxy *)
cmPerKpc = 3.08567758 * 10^21;
kgPerSunmass = 1.989 * 10^30;
JoulePerKg = (2.99792458 * 10^8)^2;
geVPerJoule = 6.24150913 * 10^9;
geVPerSunmass = kgPerSunmass * JoulePerKg * geVPerJoule;
losProjection[r_, R_] := r/Sqrt[r^2 - R^2];

generalDensityFunction[r_, r0_, ρ0_, α_, β_, γ_] := ρ0 (r/r0)^-γ (1 + (r/r0)^α)^-((β-γ)/α);

rhoDM[r_, r0_, ρ0_] = generalDensityFunction[r, r0, ρ0, αDM, βDM, γDM];
RMin = 10^-4;
RMax = 6;
r0Min = 5. * 10^-3;
r0Max = 20.;
rStarMin = 10^-3;
rStarMax = 2.;
ρ0Min = 10^5;
ρ0Max = 10^9;

SetDirectory[NotebookDirectory[]];
imported700 = << "σTableNFW_700";
σ2fun[Rx_, rStarDividedr0_] =
  Interpolation[imported700, InterpolationOrder → 3][Rx, rStarDividedr0];
σLosSquaredFullIP[R_, r0_, rStar_, ρ0_] = 2 G * ρ0 * r0^2 σ2fun[R/r0, rStar/r0];

logspace[increments_, start_?Positive, end_?Positive] :=
  Exp@Range[Log@start, Log@end, Log[end/start]/increments];


(*Looping over all Galaxies*)
```

```
For[i = 1, i ≤ Length[galaxyArray], i++,

 ClearAll[galaxy, distance, tableGalaxie, σLosSquaredRList,
  r0rStarρ0MinimizeFunction, r0rStarρ0MinimizeFunctionConst,
  minimizerStar, tableρ0r0WithTime, time, tableρ0r0, tableJ];
 galaxy = galaxyArray[[i]];

 SetDirectory[NotebookDirectory[]];
 SetDirectory["allVelocites"];
 tableGalaxy = Import[ToString@StringForm["velocities_``.dat", galaxy], "Table"];

 vLosR = Abs[tableGalaxy[[All, 2]]];
 vLosRMean = Mean[vLosR];

 σLosSquaredRList[r0_, rStar_, ρ0_] =
  tableGalaxy[[All, 3]]^2 + σLosSquaredFullIP[tableGalaxy[[All, 1]], r0, rStar, ρ0];

 r0rStarρ0MinimizeFunction[r0_, rStar_, ρ0_] = Total[
    (vLosR - vLosRMean)^2 / σLosSquaredRList[r0, rStar, ρ0] + Log[2. pi * σLosSquaredRList[r0, rStar, ρ0]]];

 r0rStarρ0MinimizeFunctionConst[r0_?NumericQ, rStar_?NumericQ, ρ0_?NumericQ] =
  Piecewise[{
    {10.^10., rStar ≤ rStarMin}, galaxy = "scl";
    {r0rStarρ0MinimizeFunction[r0, rStar, ρ0], rStar ≥ rStarMin && rStar ≤ rStarMax},
    {10.^10., rStar ≥ rStarMax}
   }];
 minimizerStar[r0_?NumericQ, ρ0_?NumericQ] :=
  FindMinimum[r0rStarρ0MinimizeFunctionConst[r0, rStar, ρ0],
   {rStar, 0.1, 0.1 + 0.01}, Method → "PrincipalAxis", WorkingPrecision → 10];

 r0Points = 7;
 ρ0Points = 7;

 r0Range = N@Range[r0Min, r0Max, (r0Max - r0Min) / r0Points];
 ρ0Range = N@logspace[ρ0Points, ρ0Min, ρ0Max];

 r0ρ0rStarL = Table[{{r0, ρ0, rStar /. minimizerStar[r0, ρ0][[2]]},
    minimizerStar[r0, ρ0][[1]]}, {r0, r0Range}, {ρ0, ρ0Range}];

 refinedr0ρ0rStarL = Select[
   Flatten[r0ρ0rStarL, 1],
   rStarMin + 0.001 < #[[1]][[3]] < rStarMax - 0.001 &
  ];

 SetDirectory[NotebookDirectory[]]
  Put[refinedr0ρ0rStarL, ToString[galaxy] <> "_r0ρ0rStarL"]
]
```

A.3 Calculate J-factors

Old J

```
ClearAll["Global`*"]
```

Profile constants

```
αDM = 1;
βDM = 3;
γDM = 1;
```

Units constants & constants

```
(* kpc, distance to galaxy *)
cmPerKpc = 3.08567758 * 10^21.;
kgPerSunmass = 1.989 * 10^30.;
JoulePerKg = (2.99792458 * 10^8)^2.;
geVPerJoule = 6.24150913 * 10^9.;
geVPerSunmass = kgPerSunmass * JoulePerKg * geVPerJoule;

pi = 3.14159265;
particelMass = 600;
G = 4.2994 * 10^-6;
```

Calculating J for a galaxy

Defining galaxy

```
galaxyArray = {"booI", "booII", "com", "cvnI", "cvnII", "dra", "her", "leoIV", "leoT",
   "seg1", "umaI", "umaII", "umi", "wil1", "car", "for", "leoI", "scl", "sex", "sgr"};
 (*"car","for","leoI","scl","sex","sgr", samtliga av dessa kan
 komma att inte fungera och ligger därför sist*)
```

Defining J

```
generalDensityFunction[r_, r0_, ρ0_, α_, β_, γ_] := ρ0 (r/r0)^-γ (1. + (r/r0)^α)^-((β-γ)/α);
rhoDM[r_, r0_, ρ0_] = generalDensityFunction[r, r0, ρ0, αDM, βDM, γDM];

θMax = 0.5/180. pi;
```

■ Get and interpolate p[vrel,x] and S[vrel]

```
For[i = 1, i ≤ Length[galaxyArray], i++,

 ClearALL[galaxy, distance, radiusFunction, r0ρ0rStarL, r0ρ0, JOld, Jold];

 galaxy = galaxyArray[[i]];

 SetDirectory[NotebookDirectory[]];
 SetDirectory["Params"];

 distance = Import[ToString@StringForm["params_``.dat", galaxy], "Table"][[2]][[1]];

 radiusFunction[s_, x_] = √(distance^2. + s^2. - 2. s distance x) ;

 JOld[r0_, ρ0_] := Log10[
   geVPerSunmass^2. * cmPerKpc^-5. *
    2. pi *

        NIntegrate[
         rhoDM[radiusFunction[s, x], r0, ρ0]^2,

         {s, 0, ∞}, {x, Cos[θMax], 1}
    ]
 ];

 SetDirectory[NotebookDirectory[]];
 SetDirectory["Minimasation"];
 r0ρ0rStarL = Get[ToString@galaxy <> "_r0ρ0rStarL"];
 r0ρ0 = Transpose[{r0ρ0rStarL[[All, 1]][[All, 1]], r0ρ0rStarL[[All, 1]][[All, 2]]}];

 Jold = Parallelize[JOld @@@ r0ρ0];

 SetDirectory[NotebookDirectory[]];
 Put[Jold, ToString@galaxy <> "_Jold"]
]
```

A.4 Dark matter velocity distribution in dSphs

Eddington Inversion

```
ClearAll["Global`*"]

pi = 3.141593;
αDM = 1.;
βDM = 3.;
γDM = 1.;
```

$$\text{generalDensityFunction}[r\_, r0\_, \rho0\_, \alpha\_, \beta\_, \gamma\_] := \rho0 \left(\frac{r}{r0}\right)^{-\gamma} \left(1 + \left(\frac{r}{r0}\right)^{\alpha}\right)^{-\frac{\beta-\gamma}{\alpha}}$$

```
rhoDM[x_] = generalDensityFunction[x, 1., 1., αDM, βDM, γDM];
(*ρ0*)

psi[x_] = 4. * pi * FullSimplify[
    1/x * Integrate[s^2 * rhoDM[s], {s, 0., x}] + Integrate[s * rhoDM[s], {s, x, ∞}]
    , x ≥ 0];
epsilonMax = Limit[psi[x], x → 0];
(*G ρ0 r0^2*)

Sqrt[8 * Limit[psi[x], x → 0]]

10.0265

rhoDMD[x] = FullSimplify[
   D[rhoDM[x], x]
  ];
(*1/r0 ρ0*)
rhoDMD2[x] = FullSimplify[
   D[rhoDM[x], {x, 2}]
  ];
(*1/r0^2 ρ0*)
psiD[x] = FullSimplify[
   D[psi[x], x]
  ];
(*G ρ0 r0*)
psiD2[x] = FullSimplify[
   D[psi[x], {x, 2}]
  ];
(*G ρ0*)

integrandEpsilonDistributionFunction[ϵ_?NumericQ, x_?NumericQ] =
  (rhoDMD[x] * psiD2[x] * psiD[x]^-2 - rhoDMD2[x] * psiD[x]^-1) /
    Sqrt[ϵ - psi[x]];
(*" (1/r0 ρ0*G ρ0* 1/(G ρ0 r0)^2 - 1/r0^2 ρ0* 1/(G ρ0 r0)) / Sqrt[G ρ0 r0^2] "*)
(* 1/(r0^3 G Sqrt[G ρ0 r0^2]) *)
```

```
Clear[epsilonDistributionFunction]

epsilonDistributionFunction[ϵ_?NumericQ] :=
  ReleaseHold[
   ReplaceAll[
     Evaluate[
      Flatten@NSolve[psi[xmin] == ϵ && xmin ≥ 0, xmin]
     ]
    ][
    Hold[

     1/Sqrt[8. pi^2] * NIntegrate[integrandEpsilonDistributionFunction[ϵ, x], {x, xmin, ∞},
       Method → {"GlobalAdaptive", "SymbolicProcessing" → 0, "SingularityDepth" →
          10000, MinRecursion → 10000, MaxRecursion → 100000}, AccuracyGoal → 5]
     ]
   ]
  ];
(*"1/(r0^3 G Sqrt[G ρ0 r0^2]) * r0"*)
(*1/(r0^2 G Sqrt[G ρ0 r0^2])*)

epsilonDistributionFunctionTable1 = Table[{ϵ^10., epsilonDistributionFunction[ϵ^10.]},
   {ϵ, (10.^-6.)^1./10., 1.^1./10., (1.^1./10. - (10.^-6.)^1./10.)/100.}] // Timing

epsilonDistributionFunctionTable2 = Table[{ϵ, epsilonDistributionFunction[ϵ]},
  {ϵ, 1., 10., 10./100.}]

epsilonDistributionFunctionTable3 = Table[{ϵ, epsilonDistributionFunction[ϵ]},
  {ϵ, 10., epsilonMax - 1./2., ((epsilonMax - 10.^-2.) - 10.)/100.}]

epsilonDistributionFunctionTable4 = Table[{ϵ, epsilonDistributionFunction[ϵ]},
  {ϵ, epsilonMax - 1./2., epsilonMax - 10.^-7.,
   ((epsilonMax - 10.^-7.) - (epsilonMax - 1./2.))/7000.}]

epsilonDistributionFunctionTable =
  Join[epsilonDistributionFunctionTable1, epsilonDistributionFunctionTable2,
   epsilonDistributionFunctionTable3, epsilonDistributionFunctionTable4];

SetDirectory[NotebookDirectory[]];
epsilonDistributionFunctionTable >> "f(ϵ)Table";

SetDirectory[NotebookDirectory[]];
epsilonDistributionFunctionTable = DeleteDuplicates[Get["fofepsilon"]];


epsilonDistributionFunctionIP = Interpolation[Re[epsilonDistributionFunctionTable]]

(*control f(ϵ)*)
Plot[Log[epsilonDistributionFunctionIP[ϵ]], {ϵ, 0, epsilonMax}]
```

RelativVelocety Distribution

Limits

```
(*[v]=√(Gρ0r0^2 *)
(*[psi[x]]=√(Gρ0r0^2 *)
upperLimitVelocityIntegral1[vRel_, x_] := √(2. psi[x]) - vRel/2.;
lowerLimitVelocityIntegral1 = 0.;
upperLimitZIntegral1 = 1.;
lowerLimitZIntegral1 = 0.;
upperLimitVelocityIntegral2[vRel_, x_] := √(8. psi[x] - vRel^2.)/2.;
lowerLimitVelocityIntegral2[vRel_, x_] := upperLimitVelocityIntegral1[vRel, x];
upperLimitZIntegral2[vRel_, vCM_?NumericQ, x_] = (8. psi[x] - vRel^2. - 4. * vCM^2.)/(4. * vCM * vRel);
lowerLimitZIntegral2 = 0.;
relativeVelocity∈Negative[vRel_?NumericQ, x_?NumericQ, vCM_?NumericQ, z_?NumericQ] =
  psi[x] - vCM^2./2. - vRel^2./8. - vCM * vRel * z/2.;
relativeVelocity∈Positive[vRel_?NumericQ, x_?NumericQ, vCM_?NumericQ, z_?NumericQ] =
  psi[x] - vCM^2./2. - vRel^2./8. + vCM * vRel * z/2.;
```

```
Clear[relativeVelocityDistribution]
relativeVelocityDistribution[vRel_?NumericQ, x_?NumericQ] := 16. pi^2. * vRel^2./rhoDM[x]^2. (

    NIntegrate[
      vCM^2. * epsilonDistributionFunctionIP[
        relativeVelocity∈Negative[vRel, x, vCM, z]
       ] *
       epsilonDistributionFunctionIP[
        relativeVelocity∈Positive[vRel, x, vCM, z]
       ],
      {vCM, lowerLimitVelocityIntegral1, upperLimitVelocityIntegral1[vRel, x]},
      {z, lowerLimitZIntegral1, upperLimitZIntegral1},

       Method →
        {"GlobalAdaptive", "SingularityDepth" → 1000000, "SymbolicProcessing" → 0},
       MinRecursion → 10, MaxRecursion → 20, AccuracyGoal → 5
      ]

      +

      NIntegrate[
       vCM^2. * epsilonDistributionFunctionIP[
         relativeVelocity∈Negative[vRel, x, vCM, z]
        ] *
        epsilonDistributionFunctionIP[
         relativeVelocity∈Positive[vRel, x, vCM, z]
        ],
       {vCM, lowerLimitVelocityIntegral2[vRel, x],
        upperLimitVelocityIntegral2[vRel, x]},
       {z, lowerLimitZIntegral2, upperLimitZIntegral2[vRel, vCM, x]},

        Method →
         {"GlobalAdaptive", "SingularityDepth" → 1000000, "SymbolicProcessing" → 0},
        MinRecursion → 10, MaxRecursion → 20, AccuracyGoal → 5
       ]
   );
(*"F[∈]"(1/(r0^2 G Sqrt[Gρ0r0^2]))^2 * "vCM"(Sqrt[Gρ0r0^2])^2 *⁝ "vRel" (Sqrt[Gρ0r0^2])^2 / "ρDM"ρ0^2  "Intgral"Sqrt[Gρ0r0^2] "?*)
(*Gρ0r0^2 * Sqrt[Gρ0r0^2] / G^2 r0^4 ρ0^2□ = Sqrt[Gρ0r0^2] / Gρ0r0^2□ *)
(*1/Sqrt[Gρ0r0^2] *)


Clear[relativeVelocityDistributionPadded]
relativeVelocityDistributionPadded[vRel_?NumericQ, x_?NumericQ] :=
 Piecewise[{{relativeVelocityDistribution[vRel, x], vRel ≤ Sqrt[8. * psi[x]]},
    {0, vRel > Sqrt[8. * psi[x]]}}]
```

```
logspace[a_, b_, n_] := 10.0^Range[Log10[a], Log10[b], (Log10[b] - Log10[a]) / (n - 1)];
vRelRange = logspace[10^-5, Sqrt[8. * epsilonMax], 50];
xRange = logspace[0.0001, 10, 50];


relativeVelocityDistributionPaddedTable =
  Table[{{vRel, x}, relativeVelocityDistributionPadded[vRel, x]},
   {vRel, vRelRange}, {x, xRange}];



SetDirectory[NotebookDirectory[]]
relativeVelocityDistributionPaddedTable1 >> "PvrelNFW_50"
```

```
/chalmers/users/michog/Desktop/kandidat
```

```
SetDirectory[NotebookDirectory[]]
relativeVelocityDistributionPaddedTable = << "PvrelNFW_50";
```

```
/chalmers/users/michog/Desktop/kandidat
```

```
p[vRel_, x_] = Interpolation[Flatten[relativeVelocityDistributionPaddedTable, 1],
   InterpolationOrder → 0][vRel, x]
```

A.5 Sommerfeld enhancement

Computation of Sommerfeld Enhancement

Declare Variables

```
ClearAll["Global`*"]
xmin = 10^-100;
mPhi = 1; (*GeV/c^2*)
alpha = 1 / 100;
b[v_, M_] := mPhi / (v * M);
a[v_] := alpha / v / 2;
stopEvaluate = 50;
logspace[increments_, start_?Positive, end_?Positive] :=
  Exp@Range[Log@start, Log@end, Log[end / start] / increments];
```

Solve S.E. and compute quantities

```
ClearAll[v, M, sol];
sol = ParametricNDSolve[
  {y''[x] + 2 / x * y'[x] + (1 + 2 * a[v] / x * Exp[-b[v, M] * x]) * y[x] == 0,
   y[xmin] == 1, y'[xmin] == -a[v]},
  y,
  {x, xmin, stopEvaluate}, {v, M}, MaxSteps → Infinity
 ]
ϕ[v_, M_, x_] = x * y[v, M][x] /. sol;
CSquaredNoLimit[v_, M_, x_] = ϕ[v, M, x]^2 + ϕ[v, M, x - π/2]^2;
CSquared[v_, M_] = CSquaredNoLimit[v, M, stopEvaluate];
Sommerfeld[v_, M_] = 1 / CSquared[v, M];
```

- Plot ψ, ϕ and C^2

```
Plot[y[10^-4, 700][x] /. sol, {x, 0, stopEvaluate}, AxesLabel → Automatic]
Plot[ϕ[10^-4, 700, x], {x, 0, stopEvaluate}, AxesLabel → Automatic]
Plot[√CSquaredNoLimit[10^-4, 700, x],
 {x, π / 2, 50}, AxesLabel → Automatic, AxesOrigin → {0, 0}]
CSquaredNoLimit[10^-4, 650, 50] / CSquaredNoLimit[10^-4, 650, 6]
```

Plot Sommerfeld for different masses

```
LogLogPlot[
 Evaluate[
  Table[
   Sommerfeld[v, i],
   {i, {600, 650, 700, 750, 800}}
  ]
 ], {v, 1/9  10^-5, 0.1},
 PlotLegends → LineLegend[{600, 650, 700, 750, 800}, LegendFunction →
    (Framed[#1, FrameMargins -> 0] &), LegendLabel → "DM Mass (GeV/c^2)"],
 AxesLabel → {"Velocity (c)", "Sommerfeld"}, ImageSize → 500,
 Frame → True, FrameStyle → Directive[Black, 16],
 FrameLabel → {Style["Relative velocity [c]", 16], Style["S(v)", 16]},
 RotateLabel → False
]
```

Plot Sommerfeld for different velocities

```
LogPlot[
 Evaluate[
  Table[
   Sommerfeld[10^i, m],
   {i, -5, -2, 1}
  ]
 ], {m, 500, 900},
 PlotLegends → LineLegend[{10^-5 c, 10^-4 c, 10^-3 c, 10^-2 c}, LegendFunction →
    (Framed[#1, FrameMargins -> 0] &), LegendLabel → "Relative Velocity"],
 AxesLabel → {"Velocity (c)", "Sommerfeld"}, AxesOrigin → {500, -10},
 ImageSize → 500, Frame → True, FrameStyle → Directive[Black, 16],
 FrameLabel → {Style["Particle Mass [GeV/c^2]", 16], Style["S(v)", 16]},
 RotateLabel → False
]
```

Check location of the resonance peak in DM Mass.

```
FindMaximum[Sommerfeld[10^-5, m], {m, 700, 710}]
```

Refine data and construct table

```
vRange = logspace[1000, 10^-8, 0.1];
M = 750;
SommerfeldTable =
  Table[{v, Sommerfeld[v, M]}, {v, vRange}] // Timing;
SetDirectory[NotebookDirectory[]];
SommerfeldTable[[2]] >> "sommerfeldTable10_3_750";
```

```
SommerfeldTable[[1]]
```

```
3.23438
```

```
SetDirectory[NotebookDirectory[]];
SommerfeldValues = << "sommerfeldTable10_3_750";

vRange = logspace[1000, 10^-8, 0.1];

SommerfeldMass = Interpolation[SommerfeldValues];
TSommerfeldValues = Transpose[SommerfeldValues];

Plot[Log10@SommerfeldMass[10^v], {v, -8, -1}]

vPad = logspace[10, 10^-8, 0.9 * 10^-6];

TSommerfeldValuesDropped =
  Map[
   Drop[
     #,
     Position[#, Max[#[[All, 2]]]][[1]][[1]]
    ] &,
   TSommerfeldValues,
   1
  ];

TSommerfeldValuesPadded =
  Map[
   PadLeft[
     #,
     {1010},
     Table[
      {
       {Flatten[{vPad, vRange}][[i]], #[[1, 1, 2]]},
       #[[1, 2]]
      },
      {i, 1, Length[Flatten@{vPad, vRange}]}
     ]
    ] &,
   TSommerfeldValuesDropped,
   1
  ];
(*Generate the sommerfeld tabel giving the interpolated function*)
TSommerfeldValuesPadded >> "SommerfeldTableComplete_750"

SommerfeldFunction = Interpolation[SommerfeldValues, InterpolationOrder → 1]

Plot[Log10@SommerfeldFunction[10^v], {v, -8, -1}]
```

A.6 Calculated J_s interpolated function

```
(*Galaxy constants*)
αDM = 1;
βDM = 3;
γDM = 1;

(*Units constants*)
cmPerKpc = 3.08567758 * 10^21.;
kgPerSunmass = 1.989 * 10^30.;
JoulePerKg = (2.99792458 * 10^8)^2.;
geVPerJoule = 6.24150913 * 10^9.;
geVPerSunmass = kgPerSunmass * JoulePerKg * geVPerJoule;

pi = 3.14159265;
particelMass = 600;
G = 4.2994 * 10^-6;


Off[NIntegrate::slwcon];
Off[NIntegrate::ncvb];
For[i = 1, i ≤ Length[galaxyArray], i++,
ClearAll[distance, radiusFunction, r0ρ0, galaxy, radiusFunction, JNew, Jnew];
  galaxy = galaxyArray1[[i]];
  SetDirectory[NotebookDirectory[]];
  SetDirectory["data"];
  SetDirectory["params"];
  distance =
   Import[ToString@StringForm["params_``.dat", galaxy], "Table"][[2]][[1]];

  radiusFunction[s_, cosθ_] = √(distance^2. + s^2. - 2. s distance cosθ) ;

  JNew[r0_, ρ0_] := Log10[
    geVPerSunmass^2. * cmPerKpc^-5.
     * 2. pi *
     1./v0[r0, ρ0] *
       NIntegrate[
        rhoDM[radiusFunction[s, x], r0, ρ0]^2. *
         gamma[v0[r0, ρ0], radiusFunction[s, x] / r0],
        {s, 0., ∞}, {x, Cos[θMax], 1.},
     Method → {"GlobalAdaptive", "SymbolicProcessing" → 0,
        "SingularityDepth" → 10000000, "MaxErrorIncreases" → 3000}, MaxRecursion → 20
     ]
   ];
  SetDirectory[NotebookDirectory[]];
  SetDirectory["Completed"];
  SetDirectory["Data"];
  SetDirectory["Minimasation"];
  r0ρ0 = Map[Drop[#, -1] &, Get[ToString[galaxy] <> "_r0ρ0rStarL"][[All, 1]]];

  Jnew = Apply[JNew, r0ρ0, {1}];
  Put[Jnew, ToString[galaxy] <> "_J_new"];
 ];
```